

**Inverse modeling of
CO₂ sources and
sinks**

R. Nassar et al.

**Inverse modeling of CO₂ sources and
sinks using satellite observations of CO₂
from TES and surface flask
measurements**

**R. Nassar^{1,*}, D. B. A. Jones¹, S. S. Kulawik², J. R. Worden², K. W. Bowman²,
R. J. Andres³, P. Suntharalingam⁴, J. M. Chen⁵, C. A. M. Brenninkmeijer⁶,
T. J. Schuck⁶, T. J. Conway⁷, and D. E. Worthy⁸**

¹Department of Physics, University of Toronto, 60 St. George Street, Toronto, Ontario, M5S 1A7, Canada

²Jet Propulsion Laboratory, California Institute of Technology, 4800 Oak Grove Drive, Pasadena CA, 91109, USA

³Environmental Sciences Division, Oak Ridge National Laboratory, Oak Ridge, TN, 37831-6335, USA

⁴Environmental Sciences, University of East Anglia, Norwich, NR4 7TJ, UK

⁵Department of Geography, University of Toronto, 45 St. George Street, Toronto, Ontario, M5S 2E5, Canada

Title Page

Abstract

Introduction

Conclusions

References

Tables

Figures

⏪

⏩

◀

▶

Back

Close

Full Screen / Esc

Printer-friendly Version

Interactive Discussion



**Inverse modeling of
CO₂ sources and
sinks**

R. Nassar et al.

[Title Page](#)[Abstract](#)[Introduction](#)[Conclusions](#)[References](#)[Tables](#)[Figures](#)[I◀](#)[▶I](#)[◀](#)[▶](#)[Back](#)[Close](#)[Full Screen / Esc](#)[Printer-friendly Version](#)[Interactive Discussion](#)

⁶ Max-Planck-Institut für Chemie, Air Chemistry Division, Mainz, Germany

⁷ Earth System Research Laboratory, National Oceanic and Atmospheric Administration, Boulder, CO, 80305-3337, USA

⁸ Climate Research Division, Environment Canada, 4905 Dufferin St., Toronto, Ontario, M3H 5T4, Canada

* now at: Climate Research Division, Environment Canada, 4905 Dufferin St., Toronto, Ontario, M3H 5T4, Canada

Received: 19 December 2010 – Accepted: 24 January 2011 – Published: 7 February 2011

Correspondence to: R. Nassar (ray.nassar@ec.gc.ca)

Published by Copernicus Publications on behalf of the European Geosciences Union.

Abstract

We infer CO₂ surface fluxes using satellite observations of mid-tropospheric CO₂ from the Tropospheric Emission Spectrometer (TES) and measurements of CO₂ from surface flasks in a time-independent inversion analysis based on the GEOS-Chem model.

5 Using TES CO₂ observations over oceans, spanning 40° S–40° N, we find that the horizontal and vertical coverage of the TES and flask data are complementary. This complementarity is demonstrated by combining the datasets in a joint inversion, which provides better constraints than from either dataset alone, when a posteriori CO₂ distributions are evaluated against independent ship and aircraft CO₂ data. In particular,
10 the joint inversion offers improved constraints in the tropics where surface measurements are sparse, such as the tropical forests of South America, which the joint inversion suggests was a weak sink of -0.17 ± 0.20 Pg C in 2006. Aggregating the annual surface-to-atmosphere fluxes from the joint inversion yields -1.13 ± 0.21 Pg C for the global ocean, -2.77 ± 0.20 Pg C for the global land biosphere and -3.90 ± 0.29 Pg C for the total global natural flux (defined as the sum of all biospheric, oceanic, and biomass burning contributions but excluding CO₂ emissions from fossil fuel combustion). These global ocean, global land and total global fluxes are shown to be in the range of other inversion results for 2006. To achieve these results, a latitude dependent bias in TES CO₂ in the Southern Hemisphere was assessed and corrected using aircraft flask data, and we demonstrate that our results have low sensitivity to variations in the bias correction approach. Overall, this analysis suggests that future carbon data assimilation systems can benefit by integrating in situ and satellite observations of CO₂ and that the vertical information provided by satellite observations of mid-tropospheric CO₂ combined with measurements of surface CO₂, provides an important additional
25 constraint for flux inversions.

Inverse modeling of CO₂ sources and sinks

R. Nassar et al.

Title Page

Abstract

Introduction

Conclusions

References

Tables

Figures

⏪

⏩

◀

▶

Back

Close

Full Screen / Esc

Printer-friendly Version

Interactive Discussion



1 Introduction

Inverse modeling has emerged as a key method for obtaining quantitative information on the global carbon cycle. In this approach, CO₂ measurements are combined with CO₂ distributions from a 3-dimensional (3-D) transport model, weighting them according to their uncertainties in order to produce optimized estimates of surface source and sink strengths (fluxes). The terrestrial biospheric flux is the component of the global carbon cycle that currently exhibits the most interannual variability, the most geographical heterogeneity and the greatest uncertainty (Denman et al., 2007, Ch.7, AR4). It is primarily responsible for the high variability in the inferred global annual mean increase of atmospheric CO₂ near the surface, which has fluctuated between 0.67 to 2.90 ppm throughout the 1980 to 2010 period (www.esrl.noaa.gov/gmd/ccgg/trends). Strong evidence suggests a link to variations in the climate system, such as the El Niño Southern Oscillation (Bacastow, 1976; Keeling et al., 1995; Heimann and Reichstein, 2008), but a thorough understanding of these mechanisms is lacking and the ability to predict future global CO₂ increases is still poor as a result of uncertainty in the strength and the spatial distribution of terrestrial CO₂ sources and sinks on regional scales. The uncertainty in surface fluxes remains a major issue for carbon cycle science, with fundamental questions such as the latitudinal distribution of natural sources and sinks still being revisited (Stephens et al., 2007).

For more than two decades, inverse modeling has been used to estimate biospheric CO₂ fluxes (e.g., Tans et al., 1989; Enting and Mansbridge, 1989, Fan et al., 1998; Rödenbeck et al., 2003; Rödenbeck, 2005; Baker et al., 2006; Deng et al., 2007; Peters et al., 2007; Chevallier et al., 2010a) using in situ observations from instruments at surface stations, towers, ships and aircraft and/or flask samples collected from these platforms, then later analyzed in a laboratory (Conway et al., 1994). Measurement coverage has increased over the years, and forward and inverse modeling techniques have also improved, but a major limitation in achieving further reductions in CO₂ flux uncertainties is the sparse data coverage that remains throughout the tropics, extra-

Inverse modeling of CO₂ sources and sinks

R. Nassar et al.

Title Page

Abstract

Introduction

Conclusions

References

Tables

Figures



Back

Close

Full Screen / Esc

Printer-friendly Version

Interactive Discussion



tropical South America and Africa, throughout Boreal Asia and the Southern Hemisphere's oceans. Figure 1 shows the stationary flask sampling locations from the National Oceanic and Atmospheric Administration (NOAA) and Environment Canada (EC) networks that collected data in 2006 (our year of investigation), along with additional ship-based and aircraft based sampling locations for that year. Although there are additional flask measurements (as well as other types of CO₂ measurements) worldwide that are made by other organizations, logistical, financial and political reasons will continue to make it difficult to develop on-site measurement or sample collection capability in remote areas such as those mentioned above. Satellite observations, therefore, offer a means to measure CO₂ without the spatial limitations of the current observing networks.

Multiple Observing System Simulation Experiments (OSSEs), which use simulated data, have explored the benefit of satellite observations of CO₂ for inverse modeling of CO₂ surface fluxes (Rayner and O'Brien, 2001; Pak and Prather, 2001; Houweling et al., 2004; Baker et al., 2006a; Chevallier et al., 2007; Miller et al., 2007; Kadygrov et al., 2009; Hungershoefer et al., 2010). Although satellite observations of CO₂ do not match the high precision of in situ or flask measurements, these studies all show that the greatly increased data coverage provided by satellites can improve CO₂ flux estimates. At the same time, it is clear that the extent to which this potential can be realized depends largely on the measurement characteristics of the different satellite instruments. CO₂ has been retrieved from spectra recorded by multiple satellite instruments, although the majority of these instruments were not originally designed for this purpose. They include the Television Infrared Observation Satellite (TIROS) Operational Vertical Sounder (TOVS) (Chédin et al., 2003), the Atmospheric Infrared Sounder (AIRS) (Chahine et al., 2008), the Tropospheric Emission Spectrometer (TES) (Kulawik et al., 2010) and the Interferometric Atmospheric Sounding Instrument (IASI) (Crevoisier et al., 2009), which measure CO₂ using thermal/mid-infrared emission and the Scanning Imaging Absorption Spectrometer for Atmospheric Chartography (SCIAMACHY) (Buchwitz et al., 2007), which measures CO₂ using near-infrared reflected

Inverse modeling of CO₂ sources and sinks

R. Nassar et al.

Title Page

Abstract

Introduction

Conclusions

References

Tables

Figures



Back

Close

Full Screen / Esc

Printer-friendly Version

Interactive Discussion



sunlight from the land surface. Few studies have inferred CO₂ surface flux estimates from real space-based CO₂ observations. Chevallier et al. (2005) was the first study, using TOVS CO₂ observations which have peak sensitivity in the upper troposphere (~150 hPa), but concluded that the retrieved surface fluxes were unrealistic. In a more recent analysis, Chevallier et al. (2009) directly assimilate AIRS radiances, but conclude that an AIRS-based CO₂ inversion performs worse than a surface flask-based inversion. The weighting functions of the AIRS radiances of Chevallier et al. (2009) are provided in Engelen et al. (2009) and show that the sensitivity to tropospheric CO₂ peaks in the upper troposphere, where the impacts of surface flux perturbations on atmospheric CO₂ are weakened by vertical transport.

New measurements from the Greenhouse Gases Observing Satellite (GOSAT) (Yokota et al., 2009; Yoshida et al., 2010) and the upcoming Orbiting Carbon Observatory 2 (OCO-2) (Crisp et al., 2004; Miller et al., 2007) offer far greater sensitivity to CO₂ near the surface by measuring near-infrared CO₂ spectral features and the O₂ A-band using sunlight reflected from Earth's surface to derive total atmospheric CO₂ columns over both land and ocean. These new satellite data are expected to improve our understanding of carbon cycle processes, especially when used in combination with the already available measurement sets with longer observational records. This concept of jointly assimilating observations from satellites and in situ data has been suggested to be the most promising method for constraining CO₂ fluxes by inverse modeling in the near future (Pak and Prather, 2001; Chevallier et al., 2009; Hungerschofer et al., 2010).

In this paper, we use the GEOS-Chem model's CO₂ simulation (Nassar et al., 2010) to examine the constraints on estimates of biospheric and oceanic fluxes of CO₂ provided by TES CO₂ observations (Kulawik et al., 2010) and surface flask measurements of CO₂ (Conway et al., 1994). TES CO₂ observation sensitivity peaks in the mid-troposphere, but because this sensitivity strongly depends on temperature, the TES CO₂ estimates are typically limited to latitudes between 40° S–40° N. Independently, TES CO₂ observations over oceans provide a weaker constraint on global CO₂ surface

Inverse modeling of CO₂ sources and sinks

R. Nassar et al.

[Title Page](#)[Abstract](#)[Introduction](#)[Conclusions](#)[References](#)[Tables](#)[Figures](#)[⏪](#)[⏩](#)[◀](#)[▶](#)[Back](#)[Close](#)[Full Screen / Esc](#)[Printer-friendly Version](#)[Interactive Discussion](#)

fluxes than data from the surface flask networks, but we demonstrate that these TES CO₂ observations can be used together with the flask data to obtain improved estimates of CO₂ surface fluxes. We find that the vertical sensitivity and horizontal coverage provided by the satellite and flask data are complementary and we show that a CO₂ flux inversion combining these data sources gives the greatest flux uncertainty reduction and the best agreement with independent ship-based and aircraft-based flask data. The integration of satellite observations of CO₂ and surface flask CO₂ data in this work is an important step toward the development of more sophisticated operational carbon assimilation systems in the future.

2 Method

Data assimilation provides a statistical framework for combining data sources with numerical models of the Earth system, weighting each according to their uncertainties. The application of this concept to inverse modeling of CO₂ fluxes involves integrating a forward model simulation and a set of observations to optimize the CO₂ fluxes at the surface. The details regarding the various components of our inverse modeling work are provided in the following subsections.

2.1 GEOS-Chem simulated CO₂

GEOS-Chem (<http://acmg.seas.harvard.edu/geos>) is a 3-D chemical transport model (Bey et al., 2001) that uses Goddard Earth Observing System (GEOS) assimilated meteorology from the NASA Global Modeling and Assimilation Office (GMAO). The original GEOS-Chem CO₂ simulation was described in Suntharalingam et al. (2004). In this work, we use version 8-02-01 with updates to the model that were presented in Nassar et al. (2010), and are now included in v8-03-02 and subsequent versions. We simulate CO₂ at a horizontal resolution of 2° latitude × 2.5° longitude with 47 vertical levels from the surface to 0.01 hPa. Our forward simulations include CO₂ fluxes

Inverse modeling of CO₂ sources and sinks

R. Nassar et al.

Title Page

Abstract

Introduction

Conclusions

References

Tables

Figures

◀

▶

◀

▶

Back

Close

Full Screen / Esc

Printer-friendly Version

Interactive Discussion



from fossil fuel combustion (including emissions from shipping and aviation), cement production, ocean processes, the terrestrial biosphere (photosynthesis, respiration, biomass/biofuel burning) and the chemical production of CO₂ from the atmospheric oxidation of other carbon species. Specific inventories used in our work are given in Table 1 and a detailed description of their implementation is given in Nassar et al. (2010), where emphasis was placed on improving anthropogenic-related inventories, since these are not optimized in our flux inversion. In the present context, biomass burning and biofuel burning are considered “natural” rather than anthropogenic fluxes, since they relate to the biosphere even though they also involve anthropogenic activity.

The use of a global inventory of national fossil fuel combustion emissions with monthly variability (Andres et al., 2011), and the 3-D representation of CO₂ emissions from aviation and the chemical production of CO₂ from the oxidation of other carbon species (CO, CH₄ and other organics) in the troposphere are unique to our CO₂ flux inversions. Since this 3-D chemical production of CO₂ (~1.05 Pg C/yr) is typically not accounted for in models, many emission inventories count CO₂ precursor species (CO, CH₄ and other carbon gases) as direct CO₂ emissions at the surface in an attempt to balance total CO₂. This leads to a reasonable estimate of total CO₂ over time, but an incorrect spatial distribution, since real chemical production of CO₂ from these species occurs at different times and locations from emission. The impact of neglecting the 3-D distribution of CO₂ from the oxidation of other carbon species on the latitudinal gradient is demonstrated in Nassar et al. (2010). Omission of this capability from CO₂ surface flux inversions has previously been shown to result in an overestimate of the northern land sink by ~0.25 Pg C/yr (Suntharalingam et al., 2005). As discussed in Nassar et al. (2010), representing the chemical production of CO₂ (~1.05 Pg C/yr) and emission of CO₂ from aviation fossil fuel use (~0.16 Pg C/yr), both of which are 3-D sources, is of increased importance when making model comparisons to CO₂ satellite observations, especially those which have peak sensitivity significantly above the surface, such as TES CO₂.

Inverse modeling of CO₂ sources and sinks

R. Nassar et al.

[Title Page](#)[Abstract](#)[Introduction](#)[Conclusions](#)[References](#)[Tables](#)[Figures](#)[⏪](#)[⏩](#)[◀](#)[▶](#)[Back](#)[Close](#)[Full Screen / Esc](#)[Printer-friendly Version](#)[Interactive Discussion](#)

Our model simulation was initialized on 1 January 2004 with a globally-uniform 3-D CO₂ field of 375 ppm. Beginning the simulation from this state allows model transport and fluxes to reproduce the large-scale features of the CO₂ distribution over time. Simulations using this approach were evaluated in Nassar et al. (2010), where it was shown that spinning up the model from this initial state produced CO₂ distributions for 2006 that were in good agreement with independent data. In order to obtain even better initial conditions for the start of the flux inversion on 1 January 2006, in the present work, we assimilated surface CO₂ data from the stationary NOAA flask sites throughout 2004 and 2005. Comparing the unconstrained model simulation and the assimilated CO₂ in 2005 with independent data comprised of over 800 ship-based flask measurements (which have a distribution very similar to that in Fig. 1) demonstrates this improvement. The 2005 annual model bias determined for all the ship-based flask measurement points was -0.37 ppm without assimilation, which is reduced to -0.15 ppm by assimilating the stationary flask observations.

2.2 TES CO₂

TES is a nadir-viewing Fourier transform spectrometer on the Aura satellite, which is at the back of the A-train in a 705 km sun-synchronous near-polar orbit with an equator crossing time of ~13:40 (Beer et al., 2001). The retrieval of TES CO₂ is described in Kulawik et al. (2010) and an example showing two months of the TES data is provided in Fig. 2. In the present work, we focus on 2006, the first full year of TES CO₂ data. Analysis of subsequent years will be carried out in future work. Since TES was not designed to produce measurements for carbon cycle science, it was not optimized for this purpose and has low sensitivity to CO₂ near the surface. TES observation sensitivity to CO₂ ranges from approximately 800 hPa to the tropopause with a peak sensitivity in the middle troposphere (near 511 hPa or 5 km altitude). Because this sensitivity strongly depends on the thermal contrast between the surface and the atmosphere, it decreases sharply poleward of 40° latitude; therefore CO₂ data beyond this latitude are not used in this work. Despite these limitations, TES CO₂ data offer a few advantages

Inverse modeling of CO₂ sources and sinks

R. Nassar et al.

Title Page

Abstract

Introduction

Conclusions

References

Tables

Figures

◀

▶

◀

▶

Back

Close

Full Screen / Esc

Printer-friendly Version

Interactive Discussion



Inverse modeling of CO₂ sources and sinks

R. Nassar et al.

Title Page

Abstract

Introduction

Conclusions

References

Tables

Figures

◀

▶

◀

▶

Back

Close

Full Screen / Esc

Printer-friendly Version

Interactive Discussion

for inverse modeling of CO₂ surface sources and sinks that are not often recognized. Firstly, the TES CO₂ retrieval peaks at a lower altitude than standard CO₂ data products from other thermal infrared sounders such as AIRS (Chahine et al., 2005) and IASI (Crevoisier et al., 2009), based on the spectral windows selected for the retrieval (Kulawik et al., 2010). As a result TES CO₂ observations should contain stronger signatures from surface fluxes. Secondly, although TES provides less global coverage than some other satellite instruments, it has the smallest footprint (5.3 × 8.3 km²) of any space-borne instrument now measuring CO₂, giving it the highest proportion of observations with negligible cloud interference. Thirdly, measurement of thermal infrared emission permits both day and night observations, which should reduce the diurnal sampling bias that is implicit to instruments measuring CO₂ using reflected sunlight such as SCIAMACHY (Buchwitz et al., 2007), the GOSAT TANSO-FTS (Yokota et al., 2009; Yoshida et al., 2010) and OCO-2 (Crisp et al., 2004; Miller et al., 2007).

The TES retrievals are reported on five pressure levels (the surface, 511, 133, 10, and 0.1 hPa), which were selected to minimize the contribution of a priori information to the retrievals, while not incurring a significant increase in vertical representation error. The retrievals are conducted with respect to the logarithm of the volume mixing ratio of CO₂ and can be expressed as a linear expansion around the a priori state x_a ,

$$\hat{x} = x_a + \mathbf{A}(x^t - x_a) + \mathbf{G}_x \varepsilon_T \quad (1)$$

where \hat{x} is the logarithm of the CO₂ profile from the TES retrieval, x^t is the logarithm of the true atmospheric CO₂ profile, \mathbf{A} is the TES averaging kernel matrix (Worden et al., 2004; Bowman et al., 2006), \mathbf{G}_x is the gain matrix and ε_T is the TES measurement noise vector. As shown in Kulawik et al. (2010), the averaging kernels peak in the mid-troposphere near 511 hPa and span ~800 hPa to lower edge of the tropopause, indicating a profile with coarse vertical resolution rather than a total column. In our analysis we, therefore, use only the retrieval values at the 511 hPa level in the retrieved profile given by Eq. (1).

The uncertainty on a single TES CO₂ observation is about 10 ppm (Kulawik et al., 2010), which primarily consists of a random component with an additional bias component. Under the assumption that the measurement uncertainty is uncorrelated between observations, the precision of N averaged observations improves according to \sqrt{N} (Daley, 1991). However, the more individual observations averaged in a bin, the fewer bins there will be for the inversion. Kulawik et al. (2010) demonstrated that for monthly-averaging at bin sizes of $10^\circ \times 10^\circ$, $15^\circ \times 15^\circ$ and $20^\circ \times 30^\circ$, the tradeoff between increased precision and a decreased number of bins nearly balances, with a very slight advantage to smaller bins. In this work, we average the TES observations at $5^\circ \times 5^\circ$ to improve precision while maintaining a high number of bins. Dealing with biases in TES CO₂ is more challenging. Biases can arise from errors in the spectroscopic parameters or from spectral lines due to other species interfering with the retrieval. In the current version of TES CO₂, a global bias correction of +2.1% was applied, which gave the best agreement with independent data (Kulawik et al., 2010), although the lack of available CO₂ data from other sources at suitable altitudes for comparison presents a challenge in quantifying TES CO₂ biases. For determining remaining biases in TES CO₂ data, we use aircraft flask measurements from the Comprehensive Observation Network for TRace gases by AirLiner (CONTRAIL) on flights between Japan and Australia (Matsueda et al., 2008; Machida et al., 2008). Although CONTRAIL data are primarily gathered at higher altitudes (~ 10 – 11 km) than the peak of TES CO₂ sensitivity (~ 5 km), they are representative of the free troposphere with minimal stratospheric influence. We have adjusted the TES CO₂ data for this work using various approaches (discussed in Sect. 3.3) based on comparisons between TES and CONTRAIL data.

The data used in this work have been filtered to remove observations with a cloud effective optical depth greater than 0.50, since thicker clouds reduce sensitivity and can contribute to biases and errors. Although TES CO₂ retrievals are carried out over both land and ocean, the retrievals over land in the current version of TES CO₂ suffer from spatially dependent biases likely due to surface silicate emissivity features in the spectra that are not accounted for in the retrievals, so in the present work, only

Inverse modeling of CO₂ sources and sinks

R. Nassar et al.

[Title Page](#)[Abstract](#)[Introduction](#)[Conclusions](#)[References](#)[Tables](#)[Figures](#)[⏪](#)[⏩](#)[◀](#)[▶](#)[Back](#)[Close](#)[Full Screen / Esc](#)[Printer-friendly Version](#)[Interactive Discussion](#)

Inverse modeling of CO₂ sources and sinks

R. Nassar et al.

[Title Page](#)[Abstract](#)[Introduction](#)[Conclusions](#)[References](#)[Tables](#)[Figures](#)[⏪](#)[⏩](#)[◀](#)[▶](#)[Back](#)[Close](#)[Full Screen / Esc](#)[Printer-friendly Version](#)[Interactive Discussion](#)

TES observations over the oceans are used. A newer version of TES CO₂ data, based on retrievals that have accounted for spectral features from silicate emissivity and other interferents, is being processed, which shows clear improvements in comparisons with independent CO₂ data. Application of this upcoming version of TES CO₂ data is expected to lead to improved CO₂ surface flux inversions, but will be left for future work. Since TES CO₂ data over land have not been used, the flask data discussed in Sect. 2.3 are the only data collected over the land used in this work, however, the ability of TES CO₂ observations over ocean to constrain terrestrial sources and sinks is discussed in Sect. 3.1.

Figure 2 shows an example of two months of 5° × 5° monthly-averaged CO₂ at 511 hPa from TES along with CO₂ simulated by GEOS-Chem. The model was sampled at the TES observation locations and times, within ±1 h, and was transformed with the TES observation operator, discussed in Sect. 2.5, to account for the low vertical resolution of the retrieval. The TES – model difference (corresponding to the difference of the two panels) is also shown. The large scale spatial patterns seen in the TES CO₂ distribution, such as the latitudinal gradient at the start of the NH growing season in May are also seen in the model CO₂ distribution; however, the model distribution is much smoother with smaller differences between maximum and minimum values.

2.3 Flask CO₂

Figure 1 illustrates the locations of the 59 National Oceanic and Atmospheric Administration Earth System Research Laboratory Global Monitoring Division (NOAA-ESRL-GMD) and Environment Canada (EC) stationary sampling sites used in this work as well as NOAA ship-based sample collection locations in the central and western Pacific Ocean, and the Drake Passage. Figure 1 also shows the sampling locations for aircraft flask CO₂ from CONTRAIL (described above) and CARIBIC (Civil Aircraft for the Regular Investigation of the atmosphere Based on an Instrument Container) (Breninkmeijer et al., 2007; Schuck et al., 2009) flights between Frankfurt, Germany and South America or Asia. These ship and aircraft flask data are not used in the inversion,

but only as an independent source of data for evaluation (ship and CARIBIC) or for correction of biases (CONTRAIL) in TES CO₂ data.

Flask samples of whole air enable highly accurate and precise measurements of CO₂ (Conway et al., 1994) in a laboratory setting. The 1-σ measurement accuracy determined from repeated analyses of CO₂ from standard gas cylinders is ~0.2 ppm. Significant effort is devoted to tracing calibration of the measurements to World Meteorological Organization (WMO) standards to put the CO₂ values on this absolute scale. The 1-σ measurement precision determined from repeated instrumental analyses of the same air sample is ~0.1 ppm. Routine intercomparisons between flask sample pairs collected in series at the same location are used to flag measurements with pair differences greater than 0.5 ppm, which have been excluded from our work. The long-term mean difference between pairs of flasks throughout the networks is ~0.2 ppm, while for 2006 (the year of this investigation), the global mean difference between pairs was ~0.1 ppm. Although the accuracy and precision of flask measurements are high, the uncertainties assigned to the data for inverse modeling are larger, since they must account for additional factors.

The observation uncertainties for the flask inversion ϵ_F are calculated using the statistics of the differences between the observations and the model simulation of the observations using the a priori emissions (e.g. Palmer et al., 2003; Heald et al., 2004)

$$\epsilon_F = \mathbf{x}_F - \mathbf{G}(\mathbf{u}) = \epsilon_f + \epsilon_r + \epsilon_m + \mathbf{b} \quad (2)$$

where ϵ_f are the flask measurement errors, ϵ_r are the representativeness errors, ϵ_m are the model errors, and \mathbf{b} is the bias. Ensuring that the errors have mean values of zero, we define the bias as the expectation of the difference between the model and observations $\mathbf{b} = \langle \mathbf{x}_F - \mathbf{G}(\mathbf{u}) \rangle$. This bias reflects the effects of systematic errors in the model transport as well as discrepancies in the a priori flux estimates in the model. The observation error covariance, therefore, is calculated as

$$\mathbf{S}^F = \left\langle (\mathbf{x}_F - \mathbf{G}(\mathbf{u}) - \mathbf{b})(\mathbf{x}_F - \mathbf{G}(\mathbf{u}) - \mathbf{b})^T \right\rangle \quad (3)$$

Inverse modeling of CO₂ sources and sinks

R. Nassar et al.

Title Page

Abstract

Introduction

Conclusions

References

Tables

Figures

◀

▶

◀

▶

Back

Close

Full Screen / Esc

Printer-friendly Version

Interactive Discussion



We neglect horizontal correlations between the flask observation locations and assume that the matrix is diagonal. Each element of the diagonal is based in the timeseries of data for 2006 at a given flask observation location. Because of the high precision of the flask data, the largest contribution to \mathbf{S}_{ii}^F comes from the representativeness error, which arises from the fact that flask measurements are essentially a point source when compared with a model grid box ($\sim 50\,000\text{ km}^2$ in this work), which has significant sub-grid variability, particularly over land in the daytime near strong flux regions (Gerbig et al., 2003a, b). In constructing the monthly averages of the flask data we do not divide by \sqrt{N} since representativeness errors do not necessarily average with more measurements due to the fact that a gridbox has some random variability and some systematic variability, although we have ensured that $\langle \epsilon_f + \epsilon_r + \epsilon_m \rangle = 0$, as required for the inversion approach. For example, the error associated with using a Mauna Loa flask measurement to represent the entire grid cell is primarily systematic and relates to properties like the sharp altitude gradient (Nassar et al., 2010).

2.4 Flux region definitions and a priori error specification

The TransCom3 project (i.e. Gurney et al., 2002; Baker et al., 2006b) divided the Earth into a set of standard regions, namely 11 land, 11 ocean and one region where zero flux is assumed (mainly consisting of Antarctica and Greenland). We use the same ocean regions but divide the land into 28 eco-regions based on geography and dominant vegetation types determined by the Advanced Very High Resolution Radiometer (AVHRR) (Hansen et al., 1998, 2000) to provide more detailed information about surface fluxes and reduce aggregation errors. An additional low-flux region consisting of Antarctica, Greenland and a few isolated islands is also defined, which we refer to as the Rest of the World (ROW). These 40 regions are explicitly identified in Kulawik et al. (2010) and are evident in Fig. 3.

We allocate uncertainties to our a priori model terrestrial biospheric fluxes based on the a posteriori uncertainties of Baker et al. (2006b), since these fluxes were used in the derivation of our terrestrial flux climatology. The Baker et al. (2006b) uncertainties

Inverse modeling of CO_2 sources and sinks

R. Nassar et al.

Title Page

Abstract

Introduction

Conclusions

References

Tables

Figures



Back

Close

Full Screen / Esc

Printer-friendly Version

Interactive Discussion



are disaggregated from 11 regions to our 28 as described in the appendix. Our a priori total biospheric flux with 1- σ uncertainty is -2.31 ± 1.26 Pg C (assuming the uncertainties are uncorrelated and applying a sum of squares approach to combine the regional uncertainties). The ocean fluxes used from Takahashi et al. (2009) were not provided with regional uncertainty estimates, but Gruber et al. (2009) carried out an ocean inversion that agreed well with the Takahashi et al. (2009) climatology, in virtually all areas except for the southern ocean. Therefore, we apply the Gruber et al. (2009) a posteriori uncertainties as our prior uncertainties in this inversion so our global total ocean flux with 1- σ uncertainty is -1.41 ± 0.33 Pg C. Since the fossil fuel combustion fluxes (including shipping and aviation) are held fixed (as in TransCom3 and most flux inversion work) and not optimized, any errors in their assumed values contribute to a posteriori errors in terrestrial biosphere and ocean fluxes. This approach is also applied to our CO₂ production from oxidation of other carbon species.

Our a priori flux uncertainties are uncorrelated, therefore our a priori error covariance matrix \mathbf{S}_a is diagonal; however, a posteriori uncertainties for land biospheric flux regions are correlated according to off-diagonal elements of the a posteriori covariance matrix that results from inversion (as in Baker et al., 2006b). As a result, the a posteriori uncertainty for the aggregation of land regions will be lower than an uncorrelated value based on summing the squares. Although, correlations could also be applied to the ocean a posteriori uncertainties, or between ocean and land regions, this avoided here since it results in unrealistically low a posteriori uncertainties for the aggregated global ocean or total global flux.

2.5 Inverse modeling approach

To quantify the CO₂ terrestrial biosphere and ocean surface fluxes we use the maximum a posteriori (MAP) approach described in Jones et al. (2003, 2009), in which we minimize the following cost function:

$$J(\mathbf{u}) = (\mathbf{x} - \mathbf{x}^m(\mathbf{u}))^T \mathbf{S}_\epsilon (\mathbf{x} - \mathbf{x}^m(\mathbf{u})) + (\mathbf{u} - \mathbf{u}_a)^T \mathbf{S}_a^{-1} (\mathbf{u} - \mathbf{u}_a) \quad (4)$$

Inverse modeling of CO₂ sources and sinks

R. Nassar et al.

Title Page

Abstract

Introduction

Conclusions

References

Tables

Figures

◀

▶

◀

▶

Back

Close

Full Screen / Esc

Printer-friendly Version

Interactive Discussion



Inverse modeling of CO₂ sources and sinks

R. Nassar et al.

Title Page

Abstract

Introduction

Conclusions

References

Tables

Figures

◀

▶

◀

▶

Back

Close

Full Screen / Esc

Printer-friendly Version

Interactive Discussion



where $\mathbf{x} = (\hat{\mathbf{x}}, \mathbf{x}_F)^T$ is the observation vector that consists of the TES CO₂ retrievals $\hat{\mathbf{x}}$ at the 511 hPa level and the flask CO₂ data at the surface \mathbf{x}_F , $\mathbf{x}^m(\mathbf{u}) = (\mathbf{F}(\mathbf{u}), \mathbf{G}(\mathbf{u}))^T$ is the model simulation of the observations, \mathbf{u} is the state vector with elements representing the CO₂ flux from the regions described in Sect. 2.5, \mathbf{u}_a is the a priori state vector, \mathbf{S}_a is the a priori covariance matrix for the fluxes, and \mathbf{S}_ε is the observation error covariance matrix. We conduct a time-independent inversion in which \mathbf{x} consists of all the monthly mean TES and flask data for 2006. Although the a priori fluxes are specified on a monthly basis, the inversion provides an optimized estimate of the annual mean fluxes. The seasonal variability of the fluxes is not adjusted in the inversion. It is used as a hard a priori constraint. The observation error consists of the TES and the flask observation errors

$$\mathbf{S}_\varepsilon = \begin{pmatrix} \mathbf{S}^T & 0 \\ 0 & \mathbf{S}^F \end{pmatrix} \quad (5)$$

where \mathbf{S}^T is the TES observation error, provided with the TES retrievals, and \mathbf{S}^F is the flask observation error. $G(\mathbf{u})$ is the forward model which reflects the transport of the CO₂ fluxes in the GEOS-Chem model, with the model sampled at the flask observation locations and times, and $\mathbf{F}(\mathbf{u})$ is the forward model that incorporates the TES observation operator (which accounts for the TES sensitivity and a priori profile as described in Eq. 1). Both the TES retrieval $\hat{\mathbf{x}}$ and the forward model simulation of the TES observations are expressed with respect to the natural logarithm of the CO₂ volume mixing ratio (VMR). The forward model $\mathbf{F}(\mathbf{u})$ is given by:

$$\mathbf{F}(\mathbf{u}) = \mathbf{x}_a + \mathbf{A}(\ln[\mathbf{H}(\mathbf{u})] - \mathbf{x}_a) \quad (6)$$

where $\mathbf{H}(\mathbf{u})$ is the modeled CO₂ profile interpolated onto the TES retrieval grid, \mathbf{x}_a is the TES a priori (given in terms of the logarithm of the CO₂ mixing ratio), and \mathbf{A} is the TES averaging kernel. Although we use only the 511 hPa level in $\mathbf{F}(\mathbf{u})$, we must transform the modeled profile using Eq. (4) to account for the vertical smoothing of the TES retrieval. Since the TES retrievals at 511 hPa have some sensitivity to

CO₂ in the lower stratosphere (Kulawik et al., 2010), and because the GEOS-Chem CO₂ simulation has not been validated in the stratosphere, we minimize the impact of biases in the modeled stratospheric CO₂ on the inversion by removing the mean bias between GEOS-Chem and TES CO₂ at 133 hPa and 10 hPa before application of the TES observation operator.

The optimal estimate or a posteriori estimate of the state vector that minimizes the cost function is given by

$$\hat{\mathbf{u}} = \mathbf{u}_a + \mathbf{S}_a \mathbf{K}^T (\mathbf{K} \mathbf{S}_a \mathbf{K}^T + \mathbf{S}_\varepsilon)^{-1} (\mathbf{x} - \mathbf{x}^m(\mathbf{u}_a)) \quad (7)$$

where $\hat{\mathbf{u}}$ is the optimized state vector and $\mathbf{K} = \partial \mathbf{x}^m(\mathbf{u}) / \partial \mathbf{u}$ is the Jacobian, which gives the sensitivity of the CO₂ abundances to the surface fluxes. We solve for Eq. (7) using the sequential update algorithm described in Jones et al. (2003). The Jacobian was estimated using separate tracers for the CO₂ from each region in the state vector. The distribution of these tracers was spun up in a 2-year run, starting on 1 January 2005, and were archived every two model hours.

3 Results and discussion

3.1 Regional flux estimates

Figure 3 shows the natural terrestrial and oceanic CO₂ flux estimates from the a priori, the flask inversion, the TES inversion, and the joint TES-Flask inversion. Values for the annual global ocean-atmosphere flux, global land-atmosphere flux and total global surface-atmosphere flux are provided on the figure. While the total annual global CO₂ flux from the a priori and the a posteriori results (the bottom number on each panel) differ by only ~8% (−3.6 to −3.9 Pg C/yr), much larger differences are seen at regional scales, specifically for the land regions. Strong sinks were a common feature in the a priori and a posteriori results for Europe, US, Mexico, Boreal Asia, Central Asia, Japan, southern Africa, Australia and New Zealand, while sources were common for Central

Inverse modeling of CO₂ sources and sinks

R. Nassar et al.

Title Page

Abstract

Introduction

Conclusions

References

Tables

Figures

◀

▶

◀

▶

Back

Close

Full Screen / Esc

Printer-friendly Version

Interactive Discussion



America and the Caribbean and the north tropical African savannas. For some regions, the a posteriori flux showed a change of sign from the a priori, such as the African tropical forest region. This region was a sink in the a priori with a flux of -0.087 ± 0.198 Pg C, but our a posteriori estimate from the joint inversion infers a weak source of 0.065 ± 0.067 Pg C. The much lower a posteriori error relative to the a priori error suggests that the TES data are providing constraints on the African tropical forest flux. Furthermore, examination of the a posteriori error correlation matrix indicates that the flux estimate from this region is not strongly correlated with estimates from other regions in the state vector, suggesting that the inversion is providing a strong constraint on the flux estimates for the African forests and that the estimated weak source inferred is likely not an artefact of the inversion. The TES and joint inversions also indicate that the North African grassland region is a strong source. This is likely a result of the seasonal biomass burning in this region which is responsible for some of the most intense fire emissions of CO₂ in the world (van der Werf, et al., 2010).

The South American tropical forest region, which primarily consists of the Amazon forests, is a strong source in the a priori (0.71 ± 0.56 Pg C), while the flask inversion suggests that it is a much weaker source (0.11 ± 0.26 Pg C). Both the TES inversion and joint inversion suggest that it is a weak sink with fluxes of -0.16 ± 0.27 Pg C and -0.17 ± 0.21 Pg C, respectively. In fact, the joint inversion shows essentially all of South America as a sink. However, the 1- σ a posteriori uncertainties in all three inversions make it difficult to distinguish whether the South American tropical forest region is a weak sink or weak source. There is considerable debate regarding the plausibility of the Amazon being a strong source of CO₂ (Stephens et al., 2007) as suggested by our a priori, but it is important to note that our a priori value was primarily based on the 1991–2000 period (Baker et al., 2006b), during which time the Amazon was believed to be a strong CO₂ source due to biomass burning and other deforestation activities that have been greatly reduced in recent years (van der Werf et al., 2010; Tollefson, 2010). Whether an Amazon sink is the new standard or whether 2006 is an anomalous year for the region related to the 2006 El Niño, recovery from the 2005 drought (Phillips

Inverse modeling of CO₂ sources and sinks

R. Nassar et al.

[Title Page](#)[Abstract](#)[Introduction](#)[Conclusions](#)[References](#)[Tables](#)[Figures](#)[⏪](#)[⏩](#)[◀](#)[▶](#)[Back](#)[Close](#)[Full Screen / Esc](#)[Printer-friendly Version](#)[Interactive Discussion](#)

et al., 2009), or re-growth from the January 2005 wind-driven tree mortality (Negrón-Juárez et al., 2010) can not be answered from a one-year inversion, but the absence of a strong net source for the Amazon in our analysis is a robust result.

Although only TES CO₂ observations over ocean were used in this work, Figure 4 shows examples of the Jacobian or sensitivity of atmospheric CO₂ near 511 hPa to the a priori fluxes for two terrestrial regions: the South American Tropical Forests and the African Tropical Forests. Monthly-averages in units of ppm CO₂ per Pg C year⁻¹ are shown. The sensitivity of the modeled CO₂ to fluxes from the South American Tropical Forest peaks at about 4 ppm/Pg C year⁻¹ over the west coast of South America and the eastern Pacific Ocean, between ~0–5° S. As shown in Fig. 2, the TES-model mismatch in this region can be as large as 5–10 ppm. For the African Tropical Forest, there are positive and negative nodes of sensitivity over the equatorial Atlantic, with somewhat lower values than from the South American Tropical forests. Jacobians for both regions illustrate that as a result of the combined horizontal and vertical transport, TES CO₂ observations over the ocean do provide sensitivity to neighbouring terrestrial surface fluxes; however, their ability to constrain these terrestrial fluxes will of course be subject to model transport biases.

The flux result for the North American Boreal forest region indicating a weak source is difficult to interpret, partly because it is for such a large area. Our approach does not reveal whether the weak source is distributed throughout the area or if it is an aggregation of smaller net source and net sink regions. Fluxes across the North American Boreal region are known to be quite heterogeneous since the ability of these forests to absorb CO₂ is linked to stand age (Pan et al., 2010), which varies across the region at various spatial scales. Furthermore, specific concentrated CO₂ sources in the boreal forest are known to occur as a result of summer drought and biomass burning (Bond-Lamberty et al., 2007) or insect infestations that have devastated some western Canadian forests, including severe mountain pine beetle infestations in 2005 and 2006 (Kurz et al., 2008). Both types of disturbances exert large impacts on the carbon balance of the affected areas, which might be enough to overcome the photosynthetic

Inverse modeling of CO₂ sources and sinks

R. Nassar et al.

[Title Page](#)[Abstract](#)[Introduction](#)[Conclusions](#)[References](#)[Tables](#)[Figures](#)[⏪](#)[⏩](#)[◀](#)[▶](#)[Back](#)[Close](#)[Full Screen / Esc](#)[Printer-friendly Version](#)[Interactive Discussion](#)

uptake of CO₂ from the forests on a regional scale, giving a net source. The region also contains Alaskan and alpine tundra that may be releasing CO₂ from permafrost thaw (Lee et al., 2010). This type of thawing is also a potential explanation for the weak source inferred for the primary North American tundra region. It is also possible that the flux estimate for one of both of these regions reflects the impact of biases in the modeled CO₂ over the North Pacific (as shown in Nassar et al., 2010), which may be linked to discrepancies in the trans-Pacific transport of Asian pollution in the model. Results for other regions of North America, such as the strong sink for the mixed forests of the east or the agricultural areas of the central US, seem much more robust with all inversions showing good agreement.

It is unclear why the TES inversion indicates that Maritime Asia (Indonesia, Malaysia, New Guinea, and The Philippines), was a sink when some of the highest levels of Indonesian biomass burning on record occurred during late 2006, related to the drought induced by El Niño and the Indian Ocean Dipole (Nassar et al., 2009). The flask inversion and the joint inversion indicate that the region was a CO₂ source, although less strongly than the prior, which is more probable than a sink. Inverse modeling studies using satellite observations of free tropospheric CO have shown that the CO source estimates for the Indonesian area are particularly sensitive to model errors (Arellano and Hess, 2006; Jiang et al., 2010). It is possible that this is also the case for inverse modeling using free tropospheric CO₂ data, which emphasizes the need for a more detailed assessment of the impact of model transport errors on inferred CO₂ fluxes (e.g., Houweling et al., 2010; Chevallier et al., 2010b), and suggests that the interpretation of the flux from any single region from these inversions should be treated with caution.

3.2 Information content

The degrees of freedom for signal d_s for the inversions, which provide a metric for the number of independent elements that are constrained, can be calculated as the trace of the inversion resolution matrix (Rodgers, 2000):

Inverse modeling of CO₂ sources and sinks

R. Nassar et al.

Title Page

Abstract

Introduction

Conclusions

References

Tables

Figures

⏪

⏩

◀

▶

Back

Close

Full Screen / Esc

Printer-friendly Version

Interactive Discussion



$$d_s = \text{tr}(\mathbf{I} - \hat{\mathbf{S}}\mathbf{S}_a^{-1}) \quad (8)$$

where \mathbf{I} is the identity matrix and $\hat{\mathbf{S}}$ is the a posteriori error covariance matrix. For the 40-element state vector, if each element were perfectly constrained, the matrix in Eq. (8) would be equal to the identity matrix and the d_s would be 40. We obtain a d_s of 22.5 for the flask inversion, 12.0 for the TES inversion and 23.7 for the joint inversion, suggesting that many of the flux regions are only partially constrained in our inversions. Since the TES data are restricted to the 40° S–40° N range, they do not provide much information on the fluxes in the middle and high latitudes and thus the d_s is much lower for the TES inversion than the flask inversion. Furthermore, since we use a strong a priori constraint on the 11 ocean regions, we would expect these inversions to produce d_s values that are significantly less than 40. It is important to note that although the d_s is a useful measure of relative information content, it is not a definitive measure, due to numerous assumptions included in the estimates of the a priori error covariance for the fluxes and the flask observation error covariance. A less restrictive specification of a priori error would result in more degrees of freedom, implying more information coming from the measurements.

3.3 Impacts of the bias correction

The sensitivity of our inversions to the bias correction approach was investigated by applying different plausible bias corrections to the TES CO₂ data and repeating the inversion. Kulawik et al. (2010) show that the current version of TES CO₂, which had a global bias correction of +2.1% applied, has a further high bias of approximately 1–2 ppm for retrievals spanning July to December located close to the CONTRAIL flight paths in the SH western Pacific. We therefore tested our joint inversion under 3 scenarios. First, with no additional correction to the bias, second, with a uniform additional correction of –1.5 ppm for 0–40° S at all longitudes for July to December, and third, with an additional bias correction based on the mean difference between TES and CONTRAIL CO₂ calculated for 10° latitude zones between 0–40° S for July to December.

Inverse modeling of CO₂ sources and sinks

R. Nassar et al.

Title Page

Abstract

Introduction

Conclusions

References

Tables

Figures

◀

▶

◀

▶

Back

Close

Full Screen / Esc

Printer-friendly Version

Interactive Discussion



The results from multiple different inversions, forming a mini-ensemble, are plotted in Fig. 5. This figure indicates that most regional flux values are relatively robust with respect to the different bias correction approaches applied since the ensemble members typically agree within their error bars, yet they often differ from the a priori values. The flux estimate for the South American tropical forest region, shown in Fig. 5, is a good example in which the joint inversion is strongly influenced by the TES observations and is in agreement with the TES inversion, while the North American Boreal Forest is a good example of a case where the joint inversions are in good agreement with the flask inversion and strongly influenced by the surface flask data. The change in size of the error bars in Fig. 5 illustrates the error reduction relative to the a priori. The greater error reduction in the joint inversion on flux estimates for regions such South America, where surface observations are sparse, can be attributed to the additional information provided by the TES observations in the tropics. In contrast, there is little change in the a posteriori uncertainties between the flask and joint inversions for the high latitudes fluxes since TES provides little information in these regions.

3.4 Comparison with other global inversions

One method of testing and comparing the overall inversion results is by aggregating the results to give global ocean, global land and global total values for the annual surface-atmosphere fluxes. These global values are given in Fig. 3, while Table 2 compares these values with some publicly available results from the Max Planck Institute for Biogeochemistry in Jena (Rödenbeck et al., 2003; Rödenbeck, 2005), la laboratoire des sciences du climat et l'environnement (LSCE) (Chevallier et al., 2005, 2010), and CarbonTracker (Peters et al., 2007, 2010). Global flux results from our inversion, the Jena v3.1 inversion and the two CarbonTracker inversions all agree within ~5% (0.17 PgC), while the global fluxes from the others agree within ~25% (1.09 PgC). The large differences in the global flux are likely attributable to the use of different fossil fuel combustion inventories (C. Rödenbeck, personal communication, 2010), which are treated as having zero error in all inversions. Total ocean-atmosphere CO₂ fluxes from these inversions differ by a factor of 5, with our a posteriori flux of -1.13 ± 0.21 PgC

Inverse modeling of CO₂ sources and sinks

R. Nassar et al.

Title Page

Abstract

Introduction

Conclusions

References

Tables

Figures

◀

▶

◀

▶

Back

Close

Full Screen / Esc

Printer-friendly Version

Interactive Discussion



as the median value and closest to the LSCE value of -1.35 Pg C. Although there is good agreement between the two CarbonTracker ocean results, they began with a similar a priori value of -2.59 ± 1.31 Pg C in 2006, which is an $\sim 85\%$ stronger sink than our value of -1.41 Pg C from Takahashi et al. (2009) with an uncertainty of ± 0.32 Pg C from Gruber et al. (2009). It should be noted that the total direct atmosphere-ocean flux is not equal to the total ocean sink, since the total ocean sink includes an additional contribution of ~ 0.45 Pg C transported to the ocean by rivers. Riverine carbon is not observed as an atmosphere-ocean flux in an atmospheric inversion but rather an atmosphere-land flux, for which the carbon is laterally transported to the ocean by rivers at a later time. Proper accounting for riverine carbon is discussed in Jacobson et al. (2007), which lists total ocean-atmosphere fluxes of -1.3 ± 1.0 to -1.9 ± 0.9 Pg C/yr obtained by various methods for 1992–1996. The magnitude of our a priori value of -1.41 Pg C for 2000 from Takahashi et al. (2009) is at the low end of this range and Takahashi et al. (2009) acknowledge potential biases in their method, suggesting that a better estimate might be -1.6 or -1.7 Pg C for 2000, while an even stronger sink can be expected for 2006.

The low magnitude of the total ocean-atmosphere flux obtained in our work can partly be attributed to the choice of a priori, which was applied with more restrictive constraints on the ocean fluxes than those for the land, based on the converging results for global atmosphere-ocean fluxes using various methods (Gruber et al., 2009). Tight constraints on a priori ocean fluxes are one method of reducing problems related to the use of only background surface sites in a traditional CO_2 flux inversion, which means that strong localized sources and sinks that are far from observations cannot be adequately constrained. Since sources tend to be more localized than sinks, their impact is systematically estimated to be dispersed over a wider scale region, attributing some component of the sources to the oceans, resulting in an erroneous ocean source term that effectively decreases the net ocean sink and increases the net land sink. This is a potential explanation for why most atmospheric inversions give weaker ocean sinks than their a priori estimates, including our flask, TES and joint inversion

Inverse modeling of CO_2 sources and sinks

R. Nassar et al.

[Title Page](#)[Abstract](#)[Introduction](#)[Conclusions](#)[References](#)[Tables](#)[Figures](#)[⏪](#)[⏩](#)[◀](#)[▶](#)[Back](#)[Close](#)[Full Screen / Esc](#)[Printer-friendly Version](#)[Interactive Discussion](#)

results, all of which represent weaker total direct ocean-atmosphere fluxes than in Jacobson et al. (2007), but are well within the error bars. The same is true of the other inversions in Table 2 and the mean of 13 separate inversions in Baker et al. (2006b), which yielded -1.06 ± 0.47 Pg C for 1991–2000 for the total ocean-atmosphere flux, compared with an a priori of -2.13 ± 0.88 Pg C. Using TES CO₂ observation near 5 km over the oceans between 40° S–40° N, as we have done means that we are still subject to this background sampling bias; however, inversions using satellite observations of CO₂ over land (i.e. from a subsequent version of the TES CO₂ retrievals or from nadir NIR observations from GOSAT or OCO-2), should not be subject to this problem.

3.5 Comparisons with independent measurements

We assess the impact of the a posteriori fluxes on the simulated CO₂ distribution using independent ship and aircraft flask measurements of atmospheric CO₂. Figure 6 shows comparisons of atmospheric CO₂ values for the entire year from the a priori, the flask a posteriori, TES a posteriori and the joint a posteriori against NOAA ship-based flask data and CARIBIC aircraft-based flask data (Fig. 1), which were not used in the inversion. Three standard goodness-of-fit metrics from a statistical analysis of variance (ANOVA), the variance (σ^2), correlation coefficient (R^2) and the F-ratio (Wilks, 2006), are provided in the figure for each comparison. For the linear regression of an independent variable x and a dependent variable y , σ^2 is a measure of how much the points spread from the regression line, R^2 can be interpreted as the proportion of the variation in y that is accounted for by the regression (ranging from 0–1), and F can be interpreted as a measure of how much the regression differs from a random distribution ($F = 1$). Therefore, a better fit is indicated by a lower σ^2 , higher R^2 , higher F and in this case also a slope closer to 1.

The comparisons with the ship-based CO₂ show that the a priori already exhibits a high level of agreement (slope = 0.942, $\sigma^2 = 0.586$ ppm, $R^2 = 0.894$, $F = 5400$) so further improvement will be challenging, yet the flask inversion improves all four metrics (slope = 0.965, $\sigma^2 = 0.455$ ppm, $R^2 = 0.919$ and $F = 7296$). In contrast, the TES

Inverse modeling of CO₂ sources and sinks

R. Nassar et al.

Title Page

Abstract

Introduction

Conclusions

References

Tables

Figures

◀

▶

◀

▶

Back

Close

Full Screen / Esc

Printer-friendly Version

Interactive Discussion



inversion produces a slight degradation in the agreement with the ship-based flask data, but combining the TES data with the stationary flask measurements in the joint inversion gives the best agreement to the ship-based flask data, with the slope increased to 1.01, the variance reduced to 0.474 ppm, the correlation increased to 0.923, and F increased to 7635. This suggests that although the TES data alone do not improve agreement with the independent surface data, they do provide useful additional information on the surface fluxes when combined with the stationary flask data.

Comparisons with CARIBIC data show that the flask inversion gives the lowest variance (0.71 ppm) but degrades the slope and the correlation of the fit. In contrast, the TES inversion improves the slope (0.87), the correlation (0.49), and the F-ratio (243) of the fit, while it degrades the agreement with respect to the variance (which increases from 0.91 to 2.7 ppm). As with the validation using the ship data, we find that integrating the TES data with the flask measurements gives the best fit to the CARIBIC data, suggesting that TES CO₂ data are indeed providing useful additional constraints on the fluxes.

The fact that the TES inversion provides the best agreement with the CARIBIC measurements near 10–11 km, whereas the flask inversion provides the best agreement with the ship-based surface flask data suggests that model transport errors are a limitation for exploiting the information that mid-tropospheric measurements can provide about the surface, or that surface measurements provide on CO₂ in the middle and upper troposphere. However, it is extremely encouraging that the combination of TES and stationary flask CO₂ provide the best overall constraint on CO₂ as seen by the comparisons with surface ship flask data based on 3 of 4 parameters (slope, R^2 and F) and with upper tropospheric aircraft data based on 2 of 4 parameters (R^2 and F). This suggests much promise in the concept of integrating satellite and surface CO₂ data in joint assimilations or inversions of surface fluxes and is perhaps an indication that in addition to the more obvious complementarity in horizontal coverage between the satellite and flask data, an additional benefit likely arises from the constraints that combining these data provide on the vertical distribution of CO₂ in the troposphere.

Inverse modeling of CO₂ sources and sinks

R. Nassar et al.

[Title Page](#)[Abstract](#)[Introduction](#)[Conclusions](#)[References](#)[Tables](#)[Figures](#)[⏪](#)[⏩](#)[◀](#)[▶](#)[Back](#)[Close](#)[Full Screen / Esc](#)[Printer-friendly Version](#)[Interactive Discussion](#)

4 Conclusions

Using the GEOS-Chem model, we have conducted a time-independent Bayesian inversion for CO₂ fluxes in 40 geographic regions, using TES CO₂ observations and measurements of CO₂ from the NOAA and Environment Canada surface flask networks for 2006. Aggregating the results for these regions, we infer a global ocean flux of -1.13 ± 0.21 Pg C, a global land biospheric flux of -2.77 ± 0.20 Pg C and total global flux of -3.90 ± 0.29 Pg C, which are in the range of other inversion results for 2006. We showed that the spatial coverage provided by satellite observations of CO₂ is an important benefit to CO₂ surface flux inversions especially in regions where the surface data are sparse such as South America or Africa. While TES CO₂ data provide weaker constraints on the surface fluxes than the flask measurements, they are shown to be complementary and combining them with the flask data produced an a posteriori CO₂ distribution that agreed best with independent ship flask measurements, as well as independent aircraft flask measurements near 10 km altitude. Since the TES data are limited to 40° S–40° N, the additional constraints on the surface fluxes were obtained mainly for the tropical regions, such as the tropical forests of South America and Africa. The joint inversion suggests that the tropical forests of South America could have been a weak sink (-0.17 ± 0.20 Pg C) in 2006, compared to the strong source assumed in the a priori ($+0.71 \pm 0.56$ Pg C). However, the uncertainty on the flux estimate is sufficiently large that it is difficult to definitively distinguish this estimate from a weak source. We also found that the joint inversion indicated that the tropical African forests are a weak source ($+0.07 \pm 0.07$ Pg C), compared to the weak sink assumed in the a priori (-0.09 ± 0.20 Pg C).

The flask inversion improved the model agreement with independent ship-based flask data, but degraded the agreement with independent aircraft data in the upper troposphere. Conversely, the TES inversion better reproduced the aircraft flask data in the upper troposphere, but exacerbated the disagreement between the model and the ship data. These different impacts of the inversions are most likely due to the influence

Inverse modeling of CO₂ sources and sinks

R. Nassar et al.

Title Page

Abstract

Introduction

Conclusions

References

Tables

Figures

⏪

⏩

◀

▶

Back

Close

Full Screen / Esc

Printer-friendly Version

Interactive Discussion



of errors in the vertical transport in the model. Although the joint inversion improved the model agreement with both datasets, our results indicate the critical need to better characterize and mitigate biases in vertical transport in the model to more accurately quantify the fluxes.

Our results also indicate that although thermal infrared observations of CO₂ have limited sensitivity near the surface, they provide useful complementary information on the horizontal and vertical distribution of CO₂ to help constrain surface fluxes when used in combination with surface data. This suggests that there is potential utility in combining thermal infrared mid-tropospheric CO₂ data with near-infrared GOSAT or OCO-2 column observations, which will be explored in future work. Although the flux estimates for many of our regions are robust, more accurate quantification will require application of more sophisticated data assimilation techniques. In particular, conducting the inversion at the resolution of the model will significantly reduce potential aggregation errors. Additional work is also needed to better characterize and improve the biases in the TES CO₂ retrievals.

Although the time-independent Bayesian analytical inversion conducted here is a somewhat simple approach, it demonstrates the value of integrating TES data with the flask measurements. Over the coming years, as CO₂ satellite observations with different vertical sensitivities and other complementary measurement characteristics become more abundant, we expect that combining these satellite observations of CO₂ along with in situ CO₂ data, using more sophisticated data assimilation systems, will significantly enhance the accuracy and precision of the inferred flux estimates. This will undoubtedly improve our understanding of the global carbon cycle, and move the field toward achieving the capability for operational monitoring of CO₂ biospheric fluxes and emissions from fossil fuel combustion for the purpose of verifying emissions for treaties that aim to limit climate change (Pacala et al., 2010).

Inverse modeling of CO₂ sources and sinks

R. Nassar et al.

Title Page

Abstract

Introduction

Conclusions

References

Tables

Figures

⏪

⏩

◀

▶

Back

Close

Full Screen / Esc

Printer-friendly Version

Interactive Discussion



Appendix A

Method for determining ocean and land region a priori uncertainties

The 30 Gruber et al. (2009) ocean region uncertainties were aggregated to our 11 TransCom regions using a sum of squares approach (which assumes that the uncertainties are uncorrelated):

$$\sigma^2 = \sum \sigma_{Gi}^2 \quad (A1)$$

where σ_{Gi} is the uncertainty on a region from Gruber et al. (2009). Using the same approach to aggregate all regions, the global ocean flux uncertainty from Gruber et al. (2009) is ± 0.32 Pg C.

We use the TransCom 3 a posteriori uncertainties from Baker et al. (2006b) that correspond to our terrestrial fluxes as the a priori uncertainties for the current inversion. The 11 TransCom 3 land regions were divided into 28 smaller regions for the present work. Partitioning the uncertainties for the regions was done by weighting them according to area and separating them using the inverse of the sum of the squares approach used for aggregating the Gruber et al. (2009) ocean flux uncertainties.

$$\sigma_{\text{Trans}}^2 = \sum_{n=1}^N \sigma_i^2 = \sum_{n=1}^N \sigma_e^2 = N \sigma_e^2 \quad (A2)$$

$$\sigma_{\text{Trans}}^2 = \sum_{n=1}^N [(1 + x_i) \sigma_e]^2 \quad (A3)$$

$$\sigma_i = (1 + x_i) \sigma_e = N \frac{A_i}{A_T} \sigma_e \quad (A4)$$

$$\frac{A_i}{A_T} = \frac{1 + x_i}{N} \quad (A5)$$

Inverse modeling of CO₂ sources and sinks

R. Nassar et al.

Title Page

Abstract

Introduction

Conclusions

References

Tables

Figures

◀

▶

◀

▶

Back

Close

Full Screen / Esc

Printer-friendly Version

Interactive Discussion



where

$$A_T = \sum_{n=1}^N A_i \quad (\text{A6})$$

N is the number of sub-regions and A_i/A_T are the ratios of the sub-region area to the full region area.

σ_e is the hypothetical uncertainty if the large region were to be subdivided into equal-area sub-regions. This can be calculated directly, then used to solve for σ_i using the fractional area ratios A_i/A_T . The x_i are positive or negative values for weighting the uncertainties. Errors for the two TransCom African regions were aggregated before subdividing since our African Tropical Forest region encompassed segments of both TransCom African regions. Similarly, uncertainties for the TransCom regions Europe and Eurasian Boreal were aggregated then divided into our 4 European and Eurasian Boreal regions (10–13) since our Eurasian Boreal Coniferous (Region 11) encompassed segments of both TransCom regions. We calculate that the aggregated TransCom a posteriori uncertainty for 11 land regions (using sums of squares which assume they are uncorrelated) is ± 1.26 Pg C/yr, which is the same as the value obtained for our aggregated 28 land regions. It should be noted that in TransCom, there is also a region 0 with no flux and no uncertainty which consists of Greenland, Antarctica, the Mediterranean and many major lakes. We define a region called the Rest of the World that also contains Greenland and Antarctica, but divide the Mediterranean between neighbouring European and Northern African regions, while lakes correspond to their surrounding land masses.

The only instances where we deviated from the above approach were for major deserts (Northern Africa and Australia) to which we allocated lower uncertainties than implied by their area, since regions with such sparse vegetation should have very low biospheric fluxes.

Inverse modeling of CO₂ sources and sinks

R. Nassar et al.

Title Page

Abstract

Introduction

Conclusions

References

Tables

Figures

◀

▶

◀

▶

Back

Close

Full Screen / Esc

Printer-friendly Version

Interactive Discussion



Acknowledgements. Work at the University of Toronto was funded by the Natural Sciences and Engineering Research Council (NSERC) of Canada. Work at the Jet Propulsion Laboratory California Institute of Technology was carried out under contract to NASA. We thank T. Machida and H. Matsueda for providing CONTRAIL CO₂ flask data for this work. Thanks to all of those who have contributed to the Carboscope (www.carboscope.eu) and CarbonTracker (www.esrl.noaa.gov/gmd/ccgg/carbontracker) websites for these excellent resources that make CO₂ flux inversion results publicly available.

References

- Andres, R. J., Gregg, J. S., Losey, L., Marland, G., and Boden, T. A.: Monthly, global emissions of carbon dioxide from fossil fuel consumption, *Tellus B*, in review, 2011.
- Arellano, A. F. and Hess, P. G.: Sensitivity of top-down estimates of CO sources to GCTM transport, *Geophys. Res. Lett.*, 33, L21807, doi:10.1029/2006GL027371, 2006.
- Bacastow, R. B.: Modulation of atmospheric carbon dioxide by the Southern Oscillation, *Nature*, 261, 116–118, 1976.
- Baker, D. F., Doney, S. C., and Schimel, D. S.: Variational data assimilation for atmospheric CO₂, *Tellus B*, 58B, 359–365, 2006a.
- Baker, D. F., Law, R. M., Gurney, K. R., Rayner, P., Peylin, P., Denning, A. S., Bousquet, P., Bruhwiler, L., Chen, Y.-H. Ciais, P., Fung, I. Y., Heimann, M., John, J., Maki, T., Maksyutov, S., Masarie, K., Prather, M., Pak, B., Taguchi, S., and Zhu, Z.: TransCom 3 inversion intercomparison: Impact of transport model errors on the interannual variability of regional CO₂ fluxes, 1988–2003, *Global Biogeochem. Cy.*, 20, GB1002, doi:10.1029/2004GB002439, 2006b.
- Beer, R., Glavich, T. A. Rider, D. M.: Tropospheric Emission Spectrometer for the Earth Observing System's Aura satellite, *Appl. Opt.*, 40, 2356–2367, 2001.
- Bey, I., Jacob, D. J., Yantosca, R. M., Logan, J. A., Field, B. D., Fiore, A. M., Li, Q. B., Liu, H. G. Y., Mickley, L. J., and Schultz, M. G.: Global modeling of tropospheric chemistry with assimilated meteorology: Model description and evaluation, *J. Geophys. Res.*, 106(D19), 23073–23095, 2001.
- Bond-Lamberty, B., Peckham, S. D., Ahl, D. E., and Gower, S. T.: Fire as the dom-

Inverse modeling of CO₂ sources and sinks

R. Nassar et al.

Title Page

Abstract

Introduction

Conclusions

References

Tables

Figures

◀

▶

◀

▶

Back

Close

Full Screen / Esc

Printer-friendly Version

Interactive Discussion



Inverse modeling of CO₂ sources and sinks

R. Nassar et al.

Title Page

Abstract

Introduction

Conclusions

References

Tables

Figures

◀

▶

◀

▶

Back

Close

Full Screen / Esc

Printer-friendly Version

Interactive Discussion

inant driver of central Canadian boreal forest carbon balance, *Nature*, 450, 89–93, doi:10.1038/nature06272, 2007.

Bowman, K. W., Rodgers, C. D., Kulawik, S. S., Worden, J., Sarkissian, E., Osterman, G., Steck, T., Lou, M., Eldering, A., Shephard, M., Worden, H., Lampel, M., Clough, S., Brown, P., Rinsland, C., Gunson, M., and Beer, R.: Tropospheric Emission Spectrometer: Retrieval method and error analysis, *IEEE T. Geosci. Remote*, 44(5), 1297–1307, 2006.

Brenninkmeijer, C. A. M., Crutzen, P., Boumard, F., Dauer, T., Dix, B., Ebinghaus, R., Filippi, D., Fischer, H., Franke, H., Frieß, U., Heintzenberg, J., Helleis, F., Hermann, M., Kock, H. H., Koepfel, C., Lelieveld, J., Leuenberger, M., Martinsson, B. G., Miemczyk, S., Moret, H. P., Nguyen, H. N., Nyfeler, P., Oram, D., O'Sullivan, D., Penkett, S., Platt, U., Pucek, M., Ramonet, M., Randa, B., Reichelt, M., Rhee, T. S., Rohwer, J., Rosenfeld, K., Scharffe, D., Schlager, H., Schumann, U., Slemr, F., Sprung, D., Stock, P., Thaler, R., Valentino, F., van Velthoven, P., Waibel, A., Wandel, A., Waschitschek, K., Wiedensohler, A., Xueref-Remy, I., Zahn, A., Zech, U., and Ziereis, H.: Civil Aircraft for the regular investigation of the atmosphere based on an instrumented container: The new CARIBIC system, *Atmos. Chem. Phys.*, 7, 4953–4976, doi:10.5194/acp-7-4953-2007, 2007.

Buchwitz, M., Schneising, O., Burrows, J. P., Bovensmann, H., Reuter, M., and Notholt, J.: First direct observation of the atmospheric CO₂ year-to-year increase from space, *Atmos. Chem. Phys.*, 7, 4249–4256, doi:10.5194/acp-7-4249-2007, 2007.

Chahine, M., Barnett, C., Olsen, E. T., Chen, L., and Maddy, E.: On the determination of atmospheric minor gases by the method of vanishing partial derivatives with application to CO₂, *Geophys. Res. Lett.*, 32(22), L22803, doi:10.1029/2005GL024165, 2005.

Chahine, M. T., Chen, L., Dimotakis, P., Jiang, X., Li, Q. B., Olsen, E. T., Pagano, T., Randerson, J., and Yung, Y. L.: Satellite remote sounding of mid-tropospheric CO₂, *Geophys. Res. Lett.*, 35(17), L17807, doi:10.1029/2008GL035022, 2008.

Chédin, A., Serrar, S., Scott, N. A., Crévoisier, C., and Armante, R.: First global measurement of midtropospheric CO₂ from NOAA polar satellites: Tropical zone, *J. Geophys. Res.*, 108(D2), 4581, doi:10.1029/2003JD003439, 2003.

Chevallier, F., Fisher, M., Peylin, P., Serrar, S., Bousquet, P., Bréon, F.-M., Chédin, A., and Ciais, P.: Inferring CO₂ sources and sinks from satellite observations: Method and application to TOVS data, *J. Geophys. Res.*, 110, D24309, doi:10.1029/2005JD006390, 2005.

Chevallier, F., Breon, F.-M., and Rayner, P. J.: Contribution of the Orbiting Carbon Observatory to the estimation of CO₂ sources and sinks: Theoretical study in a variational data assimila-

Inverse modeling of CO₂ sources and sinks

R. Nassar et al.

Title Page

Abstract

Introduction

Conclusions

References

Tables

Figures

◀

▶

◀

▶

Back

Close

Full Screen / Esc

Printer-friendly Version

Interactive Discussion



- tion framework, *J. Geophys. Res.*, 112, D09307, doi:10.1029/2006JD007375, 2007.
- Chevallier, F., Engelen, R. J., Carouge, C., Conway, T. J., Peylin, P., Pickett-Heaps, C., Ramonet, M., Rayner, P. J., and Xueref-Remy, I.: AIRS-based versus flask-based estimation of carbon surface fluxes, *J. Geophys. Res.*, 114, D20303, doi:10.1029/2009JD012311, 2009.
- 5 Chevallier, F., Ciais, P., Conway, T. J., Aalto, T., Anderson, B. E., Bousquet, P., Brunke, E. G., Ciattaglia, L., Esaki, Y., Frölich, M., Gomez, A., Gomez-Pelaez, A. J., Haszpra, L., Krummel, P. B., Langenfelds, R. L., Leuenberger, M., Machida, T., Maignan, F., Matsueda, H., Morgui, J. A., Mukai, H., Nakazawa, T., Peylin, P., Ramonet, M., Rivier, L., Sawa, Y., Schmidt, M., Steele, L. P., Vay, S. A., Vermeulen, A. T., Wofsy, S., and Worthy, D.: CO₂ surface fluxes at
- 10 grid point scale estimated from a global 21 year reanalysis of atmospheric measurements, *J. Geophys. Res.*, 115, D21307, doi:10.1029/2010JD013887, 2010a.
- Chevallier, F., Feng, L., Bösch, H., Palmer, P. I., and Rayner, P. J.: On the impact of transport model errors for the estimation of CO₂ surface fluxes from GOSAT observations, *Geophys. Res. Lett.*, 37, L21803, doi:10.1029/2010GL044652, 2010b.
- 15 Conway, T. J., Tans, P. P., Waterman, L. S., Thoning, K. W., Kitzis, D. R., Maarie, K. A., and Zhang, N.: Evidence for interannual variability of the carbon cycle from the National Oceanic and Atmospheric Administration/Climate Monitoring and Diagnostics Laboratory Global Air Sampling Network, *J. Geophys. Res.*, 99(D11), 22831–22855, 1994.
- Corbett, J. J. and Koehler, H. W.: Updated emissions from ocean shipping, *J. Geophys. Res.*, 20 108(D20), 4650, doi:10.1029/2003JD003751, 2003.
- Corbett, J. J. and Koehler, H. W.: Considering alternative input parameters in an activity-based ship fuel consumption and emissions model: Reply to comment by Øyvind Endresen et al. on “Updated emissions from ocean shipping”, *J. Geophys. Res.*, 109, D23303, doi:10.1029/2004JD005030, 2004.
- 25 Crisp, D., Atlas, R. M., Breon, F.-M., Brown, L. R., Burrows, J. P., Ciais, P., Connor, B. J., Doney, S. C., Fung, I. Y., Jacob, D. J., Miller, C. E., O’Brien, D., Pawson, S., Randerson, J. T., Rayner, P., Salawitch, R. J., Sander, S. P., Sen, B., Stephens, G. L., Tans, P. P., Toon, G. C., Wennberg, P. O., Wofsy, S. C., Yung, Y. L., Kuang, Z., Chudasama, B., Sprague, G., Weiss, B., Pollock, R., Kenyon, D., and Schroll, S.: The Orbiting Carbon Observatory (OCO) mission, *Adv. Space Res.*, 34(4), 700–709, 2004.
- 30 Crevoisier, C., Chédin, A., Matsueda, H., Machida, T., Armante, R., and Scott, N. A.: First year of upper tropospheric integrated content of CO₂ from IASI hyperspectral infrared observations, *Atmos. Chem. Phys.*, 9, 4797–4810, doi:10.5194/acp-9-4797-2009, 2009.

Daley, R.: Atmospheric Data Analysis, Cambridge University Press, 1991.

Deng, F., Chen, J., Ishizawa, M., Yuen, C.-W., Mo, G., Higuchi, K., Chan, D., and Maksyutov, S.: Global monthly CO₂ flux inversion with a focus over North America, *Tellus*, 59B, 179–190, 2007.

5 Denman, K. L., Brasseur, G., Chidthaisong, A., Ciais, P., Cox, P. M., Dickinson, R. E., hauglustaine, D., Heinze, C., Holland, E., Jacob, D., Lohmann, U., Ramachandran, S., da Silva Dias, P. L., Wofsy, S. C., and Zhang, X.: Couplings between changes in the climate system and biogeochemistry, in: *Climate Change 2007: The Physical Science Basis. Contribution of Working Group I to the Fourth Assessment Report of the Intergovernmental Panel on Climate Change*, edited by: Solomon, S., Qin, D., Manning, M., Chen, Z., Marquis, M., Averyt, K. B., Tignor, M., and Miller, H. L., Cambridge University Press, Cambridge, UK and New York, NY, USA, 2007.

10 Endresen, Ø., Sørsgård, E., Bakke, J., and Isaksen, I. S. A.: Substantiation of a lower estimate for the bunker inventory: Comment on “Updated emissions from ocean shipping” by James J. Corbett and Horst W. Koehler, *J. Geophys. Res.*, 109, D23302, doi:10.1029/2004JD004853, 2004.

15 Endresen, Ø, Sørsgård, E, Behrens, H. L., Brett, P. O., and Isaksen, I. S. A.: A historical reconstruction of ships fuel consumption and emissions, *J. Geophys. Res.*, 112, D12301, doi:10.1029/2006JD007630, 2007.

20 Enting, I. G. and Mansbridge, J. V.: Seasonal sources and sinks of atmospheric CO₂: Direct inversion of filtered data, *Tellus*, 41B, 111–126, 1989.

Engelen, R. J., Serrar, S., and Chevallier, F.: Four-dimensional data assimilation of atmospheric CO₂ using AIRS observations, *J. Geophys. Res.*, 114, D03303, doi:10.1029/2008JD010739, 2009.

25 Fan, S., Gloor, M., Mahlman, J., Pacala, S., Sarmiento, J., Takahashi, T., and Tans, P.: A Large Terrestrial Carbon Sink in North America Implied by Atmospheric and Oceanic Carbon Dioxide Data and Models, *Science*, 282, 442–446, 1998.

Friedl, R. R. (Ed.): *Atmospheric Effects of Subsonic Aircraft: Interim Assessment Report of the Advanced Subsonic Technology Program*, NASA Ref. Publ. 1400, Nat. Aeronaut. and Space Admin., Greenbelt, Md., 168 pp., 1997.

30 Gerbig, C., Lin, J. C., Wofsy, S. C. Daube, B. C., Andrews, A. E., Stephens, B. B., Bakwin, P. S., and Grainger, C. A.: Toward constraining regional-scale fluxes of CO₂ with atmospheric observations over a continent: 1. Observed spatial variability from airborne platforms, *J.*

Inverse modeling of CO₂ sources and sinks

R. Nassar et al.

Title Page

Abstract

Introduction

Conclusions

References

Tables

Figures

◀

▶

◀

▶

Back

Close

Full Screen / Esc

Printer-friendly Version

Interactive Discussion



Inverse modeling of CO₂ sources and sinks

R. Nassar et al.

Title Page

Abstract

Introduction

Conclusions

References

Tables

Figures

◀

▶

◀

▶

Back

Close

Full Screen / Esc

Printer-friendly Version

Interactive Discussion



Geophys. Res., 108(D24), 4756, doi:10.1029/2002JD003018, 2003a.

Gerbig, C., Lin, J. C., Wofsy, S. C. Daube, B. C., Andrews, A. E., Stephens, B. B., Bakwin, P. S., and Grainger, C. A.: Toward constraining regional-scale fluxes of CO₂ with atmospheric observations over a continent: 2. Analysis of COBRA data using a receptor-oriented framework, *J. Geophys. Res.*, 108(D24), 4757, doi:10.1029/2003JD003770, 2003b.

Gruber, N., Gloor, M., Mikaloff Fletcher, S. E., Doney, S. C., Dutkiewicz, S., Follows, M. J., Gerber, M., Jacobson, A. R., Joos, F., Lindsay, K., Menemenlis, D., Mouchet, A., Müller, S. A., Sarmiento, J. L., and Takahashi, T.: Oceanic sources, sinks, and transport of atmospheric CO₂, *Global Biogeochem. Cy.*, 23, GB1005, doi:10.1029/2008GB003349, 2009.

Gurney, K. R., Law, R. M., Denning, S. A., Rayner, P. J., Baker, D., Bousquet, P., Bruhwiler, L., Chen, Y.-H., Ciais, P., Fan, S., Fung, I. Y., Gloor, M., Heimann, M., Higuchi, K., John, J., Maki, T., Maksyotov, S., Masarie, K., Peylin, P., Prather, M., Pak, B. C., Randerson, J., Sarmiento, J., Taguchi, S., Takahashi, T., and Yuen, C.-W.: Towards robust regional estimates of CO₂ sources and sinks using atmospheric transport models, *Nature*, 415, 626–630, 2002.

Hansen, M. C., Defries, R. S., Townshend, J. R. G., and Sohlberg, R.: UMD Global Land Cover Classification, 1×1 degree resolution, Department of Geography, University of Maryland, College Park, Maryland, 1981–1994, 1998.

Hansen, M. C., Defries, R. S., Townshend, J. R. G., and Sohlberg, R.: Global land cover classification at 1km spatial resolution using a classification tree approach, *Int. J. Remote Sens.*, 21(6–7), 1331–1364, 2000.

Heald, C. L., Jacob, D. J., Jones, D. B. A., Palmer, P. I., Logan, J. A., Streets, D. G., Sachse, G. W., Gille, J. C., Hoffman, R. N., and Nehrkorn, T.: Comparative inverse analysis of satellite (MOPITT) and aircraft (TRACE-P) observations to estimate Asian sources of carbon monoxide, *J. Geophys. Res.*, 109, D23306, doi:10.1029/2004JD005185, 2004.

Heimann, M. and Reichstein, M.: Terrestrial ecosystem carbon dynamics and climate feedbacks, *Nature*, 451, 6591, doi:10.1038/nature06591, 2008.

Houweling, S., Breon, F.-M., Aben, I., Rödenbeck, C., Gloor, M., Heimann, M., and Ciais, P.: Inverse modeling of CO₂ sources and sinks using satellite data: a synthetic inter-comparison of measurement techniques and their performance as a function of space and time, *Atmos. Chem. Phys.*, 4, 523–538, doi:10.5194/acp-4-523-2004, 2004.

Houweling, S., Aben, I., Breon, F.-M., Chevallier, F., Deutscher, N., Engelen, R., Gerbig, C., Griffith, D., Hungershofer, K., Macatangay, R., Marshall, J., Notholt, J., Peters, W., and Serrar, S.: The importance of transport model uncertainties for the estimation of CO₂

**Inverse modeling of
CO₂ sources and
sinks**

R. Nassar et al.

Title Page

Abstract

Introduction

Conclusions

References

Tables

Figures

◀

▶

◀

▶

Back

Close

Full Screen / Esc

Printer-friendly Version

Interactive Discussion

sources and sinks using satellite measurements, *Atmos. Chem. Phys.*, 10, 9981–9992, doi:10.5194/acp-10-9981-2010, 2010.

Hungerschofer, K., Breon, F.-M., Peylin, P., Chevallier, F., Rayner, P., Klonecki, A., Houweling, S., and Marshall, J.: Evaluation of various observing systems for the global monitoring of CO₂ surface fluxes, *Atmos. Chem. Phys.*, 10, 10503–10520, doi:10.5194/acp-10-10503-2010, 2010.

Jacobson, A. R., Mikaloff-Fletcher, S. E., Gruber, N., Sarmiento, J. L., and Gloor, M.: A joint atmosphere-ocean inversion for surface fluxes of carbon dioxide: 1. Methods and global scale fluxes, *Global Biogeochem. Cy.*, 21, GB1019, doi:10.1029/2005GB002556, 2007.

Jiang, Z., Jones, D. B. A., Kopacz, M., Henze, D. K., and Heald, C.: Quantifying the impact of model errors on top-down estimates of carbon monoxide emissions using satellite observations, submitted to *J. Geophys. Res.*, 2010.

Jones, D. B. A., Bowman, K. W., Palmer, P. I., Worden, J. R., Jacob, D. J., Hoffman, R. N., Bey, I., and Yantosca, R. M.: Potential of observations from the Tropospheric Emission Spectrometer to constrain continental sources of carbon monoxide, *J. Geophys. Res.*, 108(D24), 4789, doi:10.1029/2003JD003702, 2003.

Jones, D. B. A., Bowman, K. W., Logan, J. A., Heald, C. L., Liu, J., Luo, M., Worden, J., and Drummond, J.: The zonal structure of tropical O₃ and CO as observed by the Tropospheric Emission Spectrometer in November 2004 – Part 1: Inverse modeling of CO emissions, *Atmos. Chem. Phys.*, 9, 3547–3562, doi:10.5194/acp-9-3547-2009, 2009.

Kadyrov, N., Maksyutov, S., Eguchi, N., Aoki, T., Nakazawa, T., Yokota, T. and Inoue, G.: Role of simulated GOSAT total column CO₂ observations in surface CO₂ flux uncertainty reduction, *J. Geophys. Res.*, 114, D21208, doi:10.1029/2008JD011597, 2009.

Keeling, C. D., Whorf, T. P., Whalen, M., and Vanderplicht, J.: Interannual extremes in the rate of rise of atmospheric carbon-dioxide since 1980, *Nature*, 375, 666–670, 1995.

Kim, B. Y., Fleming, G. G., Lee, J. J., Waitz, I. A., Clarke, J.-P., Balasubramanian, S., Malwitz, A., Klima, K., Locke, M., Holsclaw, C. A., Maurice, L. Q., and Gupta, M. L.: System for assessing Aviation's Global Emissions (SAGE), Part 1: Model description and inventory results, *Transportation Research Part D*, 12, 325–346, 2007.

Kulawik, S. S., Jones, D. B. A., Nassar, R., Irion, F. W., Worden, J. R., Bowman, K. W., Machida, T., Matsueda, H., Sawa, Y., Biraud, S. C., Fischer, M. L., and Jacobson, A. R.: Characterization of Tropospheric Emission Spectrometer (TES) CO₂ for carbon cycle science, *Atmos. Chem. Phys.*, 10, 5601–5623, doi:10.5194/acp-10-5601-2010, 2010.

Inverse modeling of CO₂ sources and sinks

R. Nassar et al.

Title Page

Abstract

Introduction

Conclusions

References

Tables

Figures

◀

▶

◀

▶

Back

Close

Full Screen / Esc

Printer-friendly Version

Interactive Discussion



Kurz, W. A., Dymond, C. C., Stinson, G., Rampley, G. J., Nielson, E. T., Carroll, A. L., Ebata, T., and Safranyik, L.: Mountain pine beetle and forest carbon feedback to climate change, *Nature*, 452, 987–990, doi:10.1038/nature06777, 2008.

Lee, H., Schuur, E. A. G., and Vogel, J. G.: Soil CO₂ production in upland tundra where permafrost is thawing, *J. Geophys. Res.*, 115, G01009, doi:10.1029/2008JG000906, 2010.

Machida, T., Matsueda, H., Sawa, Y., Nakagawa, Y., Hirofani, K., Kondo, N., Goto, K., Nakazawa, T., Ishikawa, K., and Ogawa, T.: Worldwide Measurements of Atmospheric CO₂ and Other Trace Gas Species Using Commercial Airlines, *J. Atmos. Ocean. Tech.*, 25(10), 1744–1754, 2008.

Matsueda, H., Machida, T., Sawa, Y., Nakagawa, Y., Hirofani, K., Ikeda, H., Kondo, N., and Goto, K.: Evaluation of atmospheric CO₂ measurements from new flask air sampling of JAL airliner observation, *Pap. Meteorol. Geophys.*, 59, 1–17, 2008.

Miller, C. E., Crisp, D., DeCola, P. L., Olsen, S. C., Randerson, J. T., Michalak, A. M., Alkhaled, Rayner, P., Jacob, D. J., Suntharalingam, P., Jones, D. B. A., Denning, A. S., Nicholls, M. E., Doney, S. C., Pawson, S., Boesh, H., Connor, B. J., Fung, I. Y., O'Brien, D., Salawitch, R. J., Sander, S. P., Sen, B., Tans, P., Toon, G. C., Wennberg, P. O., Wofsy, S. C., Yung, Y. L., and Law, R. M.: Precision requirements for space-based XCO₂ data, *J. Geophys. Res.*, 112, D10314, doi:10.1029/2006JD007659, 2007.

Nassar, R., Logan, J. A., Megretskaia, I. A., Murray, L. T., Zhang, L., and Jones, D. B. A.: Analysis of tropical tropospheric ozone, carbon monoxide and water vapor during the 2006 El Niño using TES observations and the GEOS-Chem model, *J. Geophys. Res.*, 114, D17304, doi:10.1029/2009JD011760, 2009.

Nassar, R., Jones, D. B. A., Suntharalingam, P., Chen, J. M., Andres, R. J., Wecht, K. J., Yantosca, R. M., Kulawik, S. S., Bowman, K. W., Worden, J. R., Machida, T., and Matsueda, H.: Modeling global atmospheric CO₂ with improved emission inventories and CO₂ production from the oxidation of other carbon species, *Geosci. Model Dev.*, 3, 689–716, doi:10.5194/gmd-3-689-2010, 2010.

Negrón-Juárez, R. I., Chambers, J. Q., Guimaraes, G., Zeng, H., Raupp, C. F. M., Marra, D. M., Ribeiro, G. H. P. M., Saatchi, S. S., Nelson, B. W., and Higuchi, N.: Widespread Amazon forest tree mortality from a single cross-basin squall line event, *Geophys. Res. Lett.*, 37, L16701, doi:10.1029/2010GL043733, 2010.

Olsen, S. C. and Randerson, J. T.: Differences between surface and column atmospheric CO₂ and implications for carbon cycle research, *J. Geophys. Res.*, 109, D02301,

Inverse modeling of CO₂ sources and sinks

R. Nassar et al.

Title Page

Abstract

Introduction

Conclusions

References

Tables

Figures

◀

▶

◀

▶

Back

Close

Full Screen / Esc

Printer-friendly Version

Interactive Discussion

doi:10.1029/2003JD003968, 2004.

Pacala, S., Breidenich, C., Brewer, P. G., Fung, I., Gunson, M. R., Heddle, G., Law, B., Marland, G., Paustian, K., Prather, K., Randerson, J. T., Tans, P., and Wofsy, S. C.: Verifying Greenhouse Gas Emissions: Methods to Support International Climate Agreements Committee on Methods for Estimating Greenhouse Gas Emissions, National Research Council Report, National Academies Press, Washington, DC, ISBN 978-0-309-15211-2, 2010.

Palmer, P. I., Jacob, D. J., Jones, D. B. A., Heald, C. L., Yantosca, R. M., Logan, J. A., Sachse, G. W., and Streets, D. G.: Inverting for emissions of carbon monoxide from Asia using aircraft observations over the western Pacific, *J. Geophys. Res.*, 108(D21), 8828, doi:10.1029/2003JD003397, 2003.

Pak, B. C. and Prather, M. J.: CO₂ source inversion using satellite observations in the upper troposphere, *Geophys. Res. Lett.*, 28(24) 4571–4574, 2001.

Pan, Y., Chen, J. M., Birdsey, R., McCullough, K., He, L., and Deng, F.: Age structure and disturbance legacy of North American forests, *Biogeosciences Discuss.*, 7, 979–1020, doi:10.5194/bgd-7-979-2010, 2010.

Peters, W., Jacobson, A. R., and Sweeny, C.: An atmospheric perspective on North American carbon dioxide exchange: CarbonTracker, *P. Natl. Acad. Sci.*, 104(48) 18925–18930, doi:10.1073/pnas.0708986104PNAS, 2007.

Peters, W., Krol, M. C., van der Werf, G. R., Houweling, S., Jones, C. D., Hughes, J., Schaerfer, K., Masarie, K. A., Jacobson, A. R., Miller, J. B., Cho, C. H., Ramonet, M., Schmidt, M., Ciattaglia, L., Apadula, F., Heltai, D., Meinhardt, F., di Sarra, A. G., Piacentino, S., Sferlazzo, D., Aalto, T., Hatakka, J., Ström, J., Haszpra, L., Meijer, H. A. J., van der Laan, S., Neubert, R. E. M., Jordan, A., Rodó, X., Morguá, J.-A., Vermueulen, A. T., Popa, E., Rozanski, K., Zimnoch, M., Manning, A. C., Leuenberger, M., Uglietti, C., Dolman, A. J., Ciais, P., Heimann, M., Tans, P. P.: Seven years of recent European net terrestrial carbon dioxide exchange constrained by atmospheric observations, *Glob. Change Biol.*, 16(4), 1317–1337, 2010.

Phillips, O. L., Aragão, L. E. O. C., Lewis, S. L., Fisher, J. B., Lloyd, J., López-González, G., Malhi, Y., Monteagudo, A., Peacock, J., Quesada, C. A., Van Der Heijden, G., Almeida, S., Amaral, I., Arroyo, L., Aymard, G., Baker, T. R., Bánki, O., Blanc, L., Bonal, D., Brando, P., Chave, J., De Oliveira, A. C. A., Cardozo, N. D., Czimczik, C. I., Feldpausch, T. R., Freitas, M. A., Gloor, E., Higuchi, N., Jiménez, E., Lloyd, G., Meir, P., Mendoza, C., Morel, A., Neill, D. A., Nepstad, D., Patiño, S., Peñuela, M. C. Prieto, A., Ramírez, F., Schwarz, M., Silva, J., Silveira, M., Thomas, A. S., Steege, H. T., Stropp, J., Vásquez, R., Zelazowski, P., Dávila, E.

Inverse modeling of CO₂ sources and sinks

R. Nassar et al.

Title Page

Abstract

Introduction

Conclusions

References

Tables

Figures

◀

▶

◀

▶

Back

Close

Full Screen / Esc

Printer-friendly Version

Interactive Discussion



A., Andelman, S., Andrade, A., Chao, K.-J., Erwin, T., Di Fiore, A., Honorio, E. C., Keeling, H., Killeen, T., Laurance, W. F., Cruz, A. P., Pitman, N. C. A., Vargas, P. N., Ramírez-Angulo, H., Rudas, A., Salamão, R., Silva, N., Terborgh, J., Torres-Lezama, Á.: Drought Sensitivity of the Amazon Rainforest, *Science*, 323, 1344–1347, 2009.

5 Rayner, P. J. and O'Brien, D. M.: The utility of remotely sensed CO₂ concentration data in surface source inversions, *Geophys. Res. Lett.*, 28(1), 175–178, 2001.

Rödenbeck, C., Houweling, S., Gloor, M., and Heimann, M.: CO₂ flux history 1982–2001 inferred from atmospheric data using a global inversion of atmospheric transport, *Atmos. Chem. Phys.*, 3, 1919–1964, doi:10.5194/acp-3-1919-2003, 2003.

10 Rödenbeck, C.: Estimating CO₂ sources and sinks from atmospheric mixing ratio measurements using a global inversion of atmospheric transport, Technical Report, Max-Planck-Institut für Biogeochemie, Technical Reports 6, ISSN 1615-7400, 2005.

Rodgers, C. D.: *Inverse methods for Atmospheric Sounding: Theory and Practice*, World Scientific, Singapore, 2000.

15 Schuck, T. J., Brenninkmeijer, C. A. M., Slemr, F., Xueref-Remy, I., and Zahn, A.: Greenhouse gas analysis of air samples collected onboard the CARIBIC passenger aircraft, *Atmos. Meas. Tech.*, 2, 449–464, doi:10.5194/amt-2-449-2009, 2009.

Stephens, B. B., Gurney, K. R., Tans, P. P., Sweeney, C., Peters, W., Bruhwiler, L., Ciais, P., Ramonet, M., Bousquet, P., Nakazawa, T., Aoki, S., Machida, T., Inoue, G., Vinnichenko, N., Lloyd, J., Jordan, A., Heimann, M., Shibistova, O., Langenfelds, R. L., Steele, L. P., Francey, R. J., and Denning, A. S.: Weak northern and strong tropical land carbon uptake from vertical profiles of atmospheric CO₂, *Science*, 316(5832), 1732–1735, 2007.

20 Suntharalingam, P., Jacob, D. J., Palmer, P. I., Logan, J. A., Yantosca, R. M., Xiao, Y., Evans, M. J., Streets, D. G., Vay, S. L., and Sachse, G. W.: Improved quantification of Chinese carbon fluxes using CO₂/CO correlations in Asian outflow, *J. Geophys. Res.*, 109, D18S18, doi:10.1029/2003JD004362, 2004.

25 Suntharalingam, P., Randerson, J. T., Krakauer, N., Logan, J. A., and Jacob, D. J.: Influence of reduced carbon emissions and oxidation on the distribution of atmospheric CO₂: Implications for inversion analyses, *Global Biogeochem. Cy.*, 19, GB4003, doi:10.1029/2005GB002466, 2005.

30 Takahashi, T., Sutherland, S. C., Wanninkhof, R., Sweeney, C., Feely, R. A., Chipman, D. W., Hales, B., Friederich, G., Chavez, F., Sabine, C., Watson, A., Bakker, D. C. E., Schuster, U., Metzl, N., Yoshikawa-Inoue, H., Ishii, M., Midorikawa, T., Nojiri, Y., Körtzinger, A., Steinhoff,

Inverse modeling of CO₂ sources and sinks

R. Nassar et al.

Title Page

Abstract

Introduction

Conclusions

References

Tables

Figures

◀

▶

◀

▶

Back

Close

Full Screen / Esc

Printer-friendly Version

Interactive Discussion



T., Hoppema, M., Olafsson, J., Arnarson, T. S., Tilbrook, B., Johannessen, T., Olsen, A., Bellerby, R., Wong, C. S., Delille, B., Bates, N. R., and de Baar, H. J. W.: Climatological mean and decadal change in surface ocean pCO₂, and net sea-air CO₂ flux over the global oceans, *Deep-Sea Res. II*, 56(8–10), 554–577, doi:10.1016/j.dsr2.2008.12.009, 2009.

5 Tans, P. P., Conway, T. J., and Nakazawa, T: Latitudinal distribution of the sources and sinks of atmospheric carbon dioxide derived from surface observations and an atmospheric transport model, *J. Geophys. Res.*, 94, 5151–5172, 1989.

Tollefson, J.: Climate talks focus on lesser goals, *Nature*, 468, 488–489, doi:10.1038/468488a, 2010.

10 van der Werf, G. R., Randerson, J. T., Giglio, L., Collatz, G. J., Kasibhatla, P. S., and Arellano Jr., A. F.: Interannual variability in global biomass burning emissions from 1997 to 2004, *Atmos. Chem. Phys.*, 6, 3423–3441, doi:10.5194/acp-6-3423-2006, 2006.

van der Werf, G. R., Randerson, J. T., Giglio, L., Collatz, G. J., Mu, M., Kasibhatla, P. S., Morton, D. C., DeFries, R. S., Jin, Y., and van Leeuwen, T. T.: Global fire emissions and the contribution of deforestation, savanna, forest, agricultural, and peat fires (1997–2009), *Atmos. Chem. Phys.*, 10, 11707–11735, doi:10.5194/acp-10-11707-2010, 2010.

15 Wilkerson, J. T., Jacobson, M. Z., Malwitz, A., Balasubramanian, S., Wayson, R., Fleming, G., Naiman, A. D., and Lele, S. K.: Analysis of emission data from global commercial aviation: 2004 and 2006, *Atmos. Chem. Phys.*, 10, 6391–6408, doi:10.5194/acp-10-6391-2010, 2010.

20 Wilks, D. S.: *Statistical Methods in the Atmospheric Sciences* (2nd ed), Elsevier, Amsterdam, 2006.

Worden, J., Kulawik, S. S., Shephard, M. W., Clough, S. A., Worden, H., Bowman, K., and Goldman, A.: Predicted errors of tropospheric emission spectrometer nadir retrievals from spectral window selection, *J. Geophys. Res.-Atmos.*, 109(D9), D09308, doi:10.1029/2004JD004522, 2004.

25 Yevich, R. and Logan, J. A.: An assessment of biofuel use and burning of agricultural waste in the developing world, *Global Biogeochem. Cy.*, 17(4), 1095, doi:10.1029/2002GB001952, 2003.

30 Yokota, T., Yoshida, Y., Eguchi, N., Ota, Y., Tanaka, T., Watanabe, H., and Maksyutov, S.: Global Concentrations of CO₂ and CH₄ Retrieved from GOSAT: first Preliminary Results, *Sci. Online Lett. Atmos.*, 5, 160–163, doi:10.2151/sola.2009-041, 2009.

Yoshida, Y., Ota, Y., Eguchi, N., Kikuchi, N., Nobuta, K., Tran, H., Morino, I., and Yokota, T.:

Retrieval algorithm for CO₂ and CH₄ column abundances from short-wavelength infrared spectral observations by the Greenhouse Gases Observing Satellite, Atmos. Meas. Tech. Discuss., 3, 4791–4833, doi:10.5194/amtd-3-4791-2010, 2010.

Discussion Paper | Discussion Paper | Discussion Paper | Discussion Paper | Discussion Paper

ACPD

11, 4263–4311, 2011

Inverse modeling of CO₂ sources and sinks

R. Nassar et al.

Title Page

Abstract

Introduction

Conclusions

References

Tables

Figures



Back

Close

Full Screen / Esc

Printer-friendly Version

Interactive Discussion



Table 1. Summary of emission inventories used in our GEOS-Chem CO₂ model simulation. The first 4 inventories are held fixed and not optimized in the inversion. The last 5 inventories are used only as the a priori for natural fluxes from the terrestrial biosphere and oceans.

Flux Type	Inventory Name	Description	2006 Global Annual Flux	References
National fossil fuel and cement manufacture	Carbon Dioxide Information Analysis Center (CDIAC) 1°×1° monthly	1°×1° monthly fossil fuel and cement manufacture CO ₂ emissions from national totals (excludes international bunker fuels)	8.23 Pg C	Andres et al. (2011)
Shipping	International Comprehensive Ocean-Atmosphere Data Set (ICOADS)	0.1°×0.1° monthly shipping emissions of CO ₂ , scaled to 2006	0.19 Pg C	Corbett and Koehler (2003, 2004) Endresen et al. (2004, 2007)
Aviation	Atmospheric Effects of Aviation Project (AEAP) and System for Assessing Aviation Emissions (SAGE)	2°×2.5° gridded flight track density based on Friedl (1997) used for GEOS-Chem sulfate simulation, scaled to 2006 for aviation CO ₂ emissions	0.16 Pg C	Friedl (1997), Kim et al. (2007), Wilkerson et al. (2010)
Chemical Source	GEOS-Chem CO ₂ Chemical Source	Chemical production of CO ₂ based on CO loss rates from GEOS-Chem 4°×5° simulations	1.05 Pg C	Nassar et al. (2010)
Residual Annual Terrestrial Exchange	TransCom climatology	1°×1° annual climatology based on TransCom CO ₂ inversion results adjusted with GFEDv2 fire emissions	-5.29 Pg C	Baker et al. (2006b), van der Werf et al. (2006)
Biomass Burning	Global Fire Emission Database (GFED) v2	1°×1° biomass burning CO ₂ emissions (8-day averages)	2.16 Pg C	van der Werf et al. (2006)
Biofuel Burning	Yevich and Logan	1°×1° annual inventory of biofuel (heating/cooking) CO ₂ emissions for 1985 and scaled to 1995, excluding burning in agricultural fields	0.80 Pg C	Yevich and Logan (2003)
Balanced Biosphere	Careneegie Ames Stanford Approach (CASA) balanced biosphere diurnal fluxes	1°×1° 3-hourly Net Ecosystem Productivity (NEP) for 2000	0.00 Pg C	Olsen and Randerson (2004)
Ocean Exchange	Takahashi et al. (2009)	4°×5° climatology of monthly ocean-atmosphere CO ₂ flux	-1.41 Pg C	Takahashi et al. (2009)

Inverse modeling of CO₂ sources and sinks

R. Nassar et al.

Title Page

Abstract

Introduction

Conclusions

References

Tables

Figures



Back

Close

Full Screen / Esc

Printer-friendly Version

Interactive Discussion



Inverse modeling of CO₂ sources and sinks

R. Nassar et al.

Title Page

Abstract

Introduction

Conclusions

References

Tables

Figures

⏪

⏩

◀

▶

Back

Close

Full Screen / Esc

Printer-friendly Version

Interactive Discussion



Table 2. Aggregated inversion values (Pg C) from the current work compared with publicly available results for 2006.

Inversion	Global Ocean	Global Land	Global Total
TES-Flask-GEOS-Chem (<i>this work</i>)	−1.13	−2.77	−3.90
LSCE v1.0 ^a	−1.35	−3.26	−4.79
Jena v3.1 ^{a,b}	−0.51	−3.45	−3.96
Jena v3.2 s96 ^{a,b}	−0.45	−4.46	−4.99
Jena v3.2 s99 ^{a,b}	−0.43	−4.42	−4.92
CarbonTracker-EU v2008 ^{a,c}	−2.35	−1.60	−3.95
CarbonTracker-NOAA v2009 ^c	−2.26	−1.81	−4.07

^a www.carboscope.eu

^b www.bgc-jena.mpg.de/~christian.roedenbeck/download-CO2/

^c www.esrl.noaa.gov/gmd/ccgg/carbontracker

Inverse modeling of CO₂ sources and sinks

R. Nassar et al.

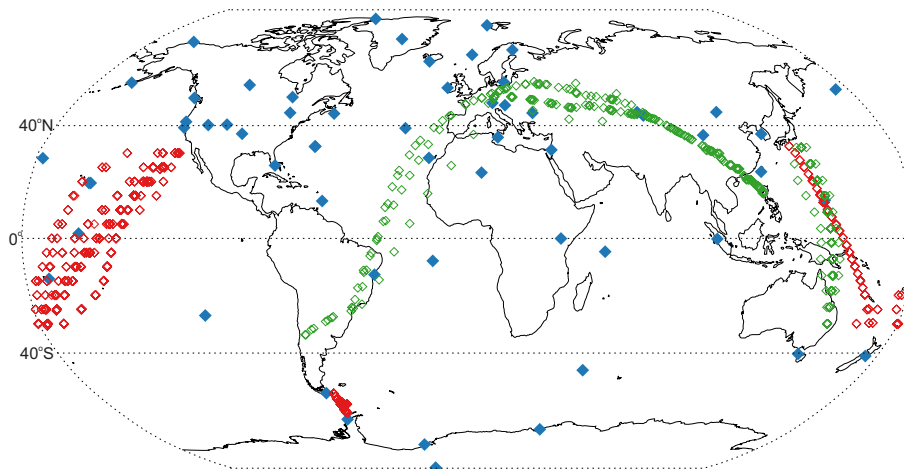


Fig. 1. Global distribution of CO₂ flask sample collection locations from the 59 stationary surface sites of NOAA and Environment Canada spanning 90° S–82° N (blue solid symbols), NOAA ship-based sampling locations in the Pacific Ocean and Drake Passage (red open symbols) and aircraft sampling locations from CARIBIC and CONTRAIL (green open symbols). TES observations of CO₂ span the 40° S–40° N range denoted by the dotted lines.

[Title Page](#)[Abstract](#)[Introduction](#)[Conclusions](#)[References](#)[Tables](#)[Figures](#)[◀](#)[▶](#)[◀](#)[▶](#)[Back](#)[Close](#)[Full Screen / Esc](#)[Printer-friendly Version](#)[Interactive Discussion](#)

Inverse modeling of
CO₂ sources and
sinks

R. Nassar et al.

Title Page

Abstract

Introduction

Conclusions

References

Tables

Figures



Back

Close

Full Screen / Esc

Printer-friendly Version

Interactive Discussion

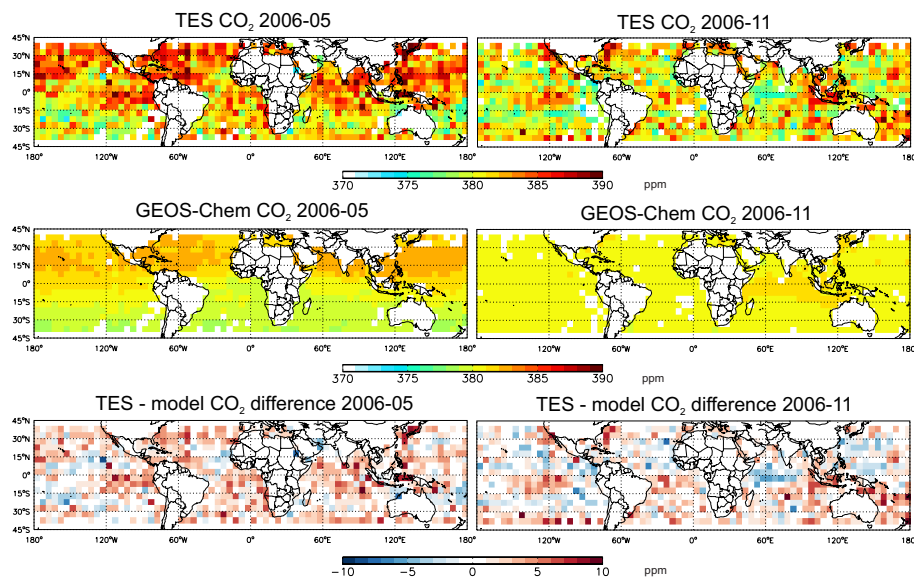


Fig. 2. Monthly-averaged $5^\circ \times 5^\circ$ TES CO₂ (ppm) near 511 hPa (top), GEOS-Chem CO₂ at the equivalent model level sampled at the TES observation locations and times (± 1 h) with the TES averaging kernel and constraint applied (middle), and the TES minus model difference (bottom) for May and November 2006. As a result of the seasonal cycle, the latitudinal gradient of CO₂ is strongest in May, while it is absent in November for both TES and the model (with the TES averaging kernel and constraint applied).

Inverse modeling of CO₂ sources and sinks

R. Nassar et al.

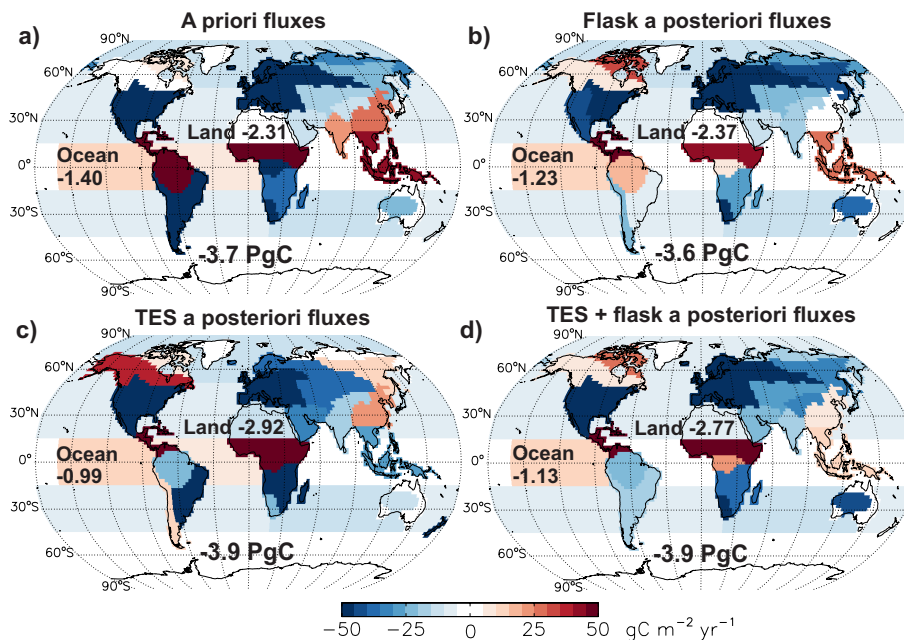


Fig. 3. (a) A priori CO₂ fluxes and flux estimates from the (b) flask inversion, (c) TES inversion and d) combined (TES + flask) inversion. The aggregated ocean, aggregated land and global total annual CO₂ flux values in PgC for the year 2006 are shown for each panel.

Title Page

Abstract

Introduction

Conclusions

References

Tables

Figures

◀

▶

◀

▶

Back

Close

Full Screen / Esc

Printer-friendly Version

Interactive Discussion



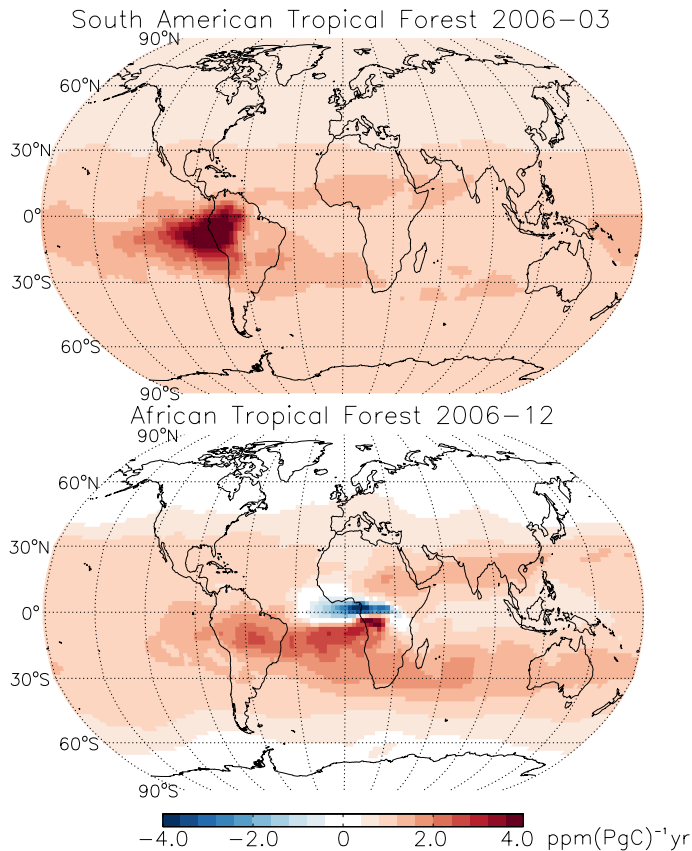


Fig. 4. Examples of Jacobians or sensitivity functions for the biospheric fluxes from South American Tropical Forest and the African Tropical Forest regions, which can be seen in Fig. 3. The location of the peak intensity of the Jacobians indicates that TES CO₂ observations over the oceans will contain information about terrestrial surface fluxes, but this will be subject to transport biases.

Inverse modeling of CO₂ sources and sinks

R. Nassar et al.

Title Page

Abstract

Introduction

Conclusions

References

Tables

Figures

◀

▶

◀

▶

Back

Close

Full Screen / Esc

Printer-friendly Version

Interactive Discussion

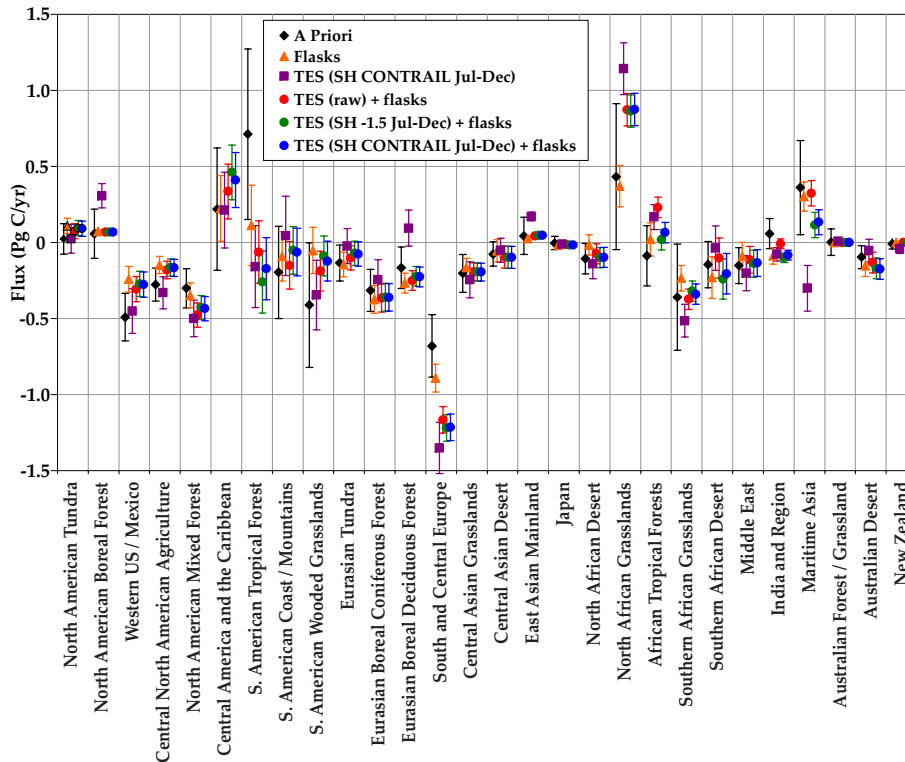


Fig. 5. Mini-ensemble of a posteriori fluxes compared with the a priori for the 28 land regions. Error bars denote the 1- σ flux uncertainty. Different treatments of the bias change the exact numbers but the differences typically remain within the error bars. The region for which the a posteriori flux differs most from the a priori is the South American tropical forest region, which is consistently a sink in all inversions that include TES CO₂ data and nearly neutral in the flask-only inversion.

Inverse modeling of CO₂ sources and sinks

R. Nassar et al.

Title Page

Abstract Introduction

Conclusions References

Tables Figures

◀ ▶

◀ ▶

Back Close

Full Screen / Esc

Printer-friendly Version

Interactive Discussion



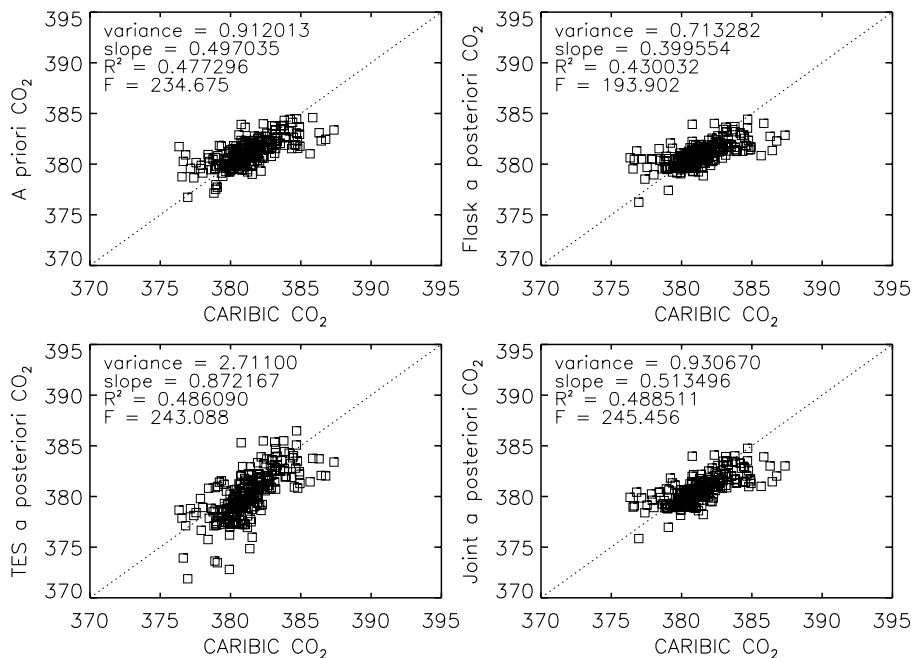


Fig. 6a. Scatter plots comparing a priori CO_2 with a posteriori CO_2 from the flask-based, the TES-based and the joint (TES and flask) inversions with CO_2 measurements from CARIBIC (aircraft) and ship-based flasks for 2006. The ship and aircraft data were not used in the assimilation. The slope, variance, correlation coefficient (R^2) and F-ratio are provided for each panel as metrics for gauging the agreement. Independently assimilating TES CO_2 data improves the agreement with aircraft data (based on the slope and F) but degrades the agreement with the ship-based data (based on all metrics), while independently assimilating the flask data degrades the agreement with aircraft data (based on 3 of 4 metrics) and improves the agreement with the ship-based data (based on all metrics). The joint assimilation gives the best agreement with both the aircraft data (based on R^2 and F) and ship-based data sets (based on 3 metrics).

Inverse modeling of CO_2 sources and sinks

R. Nassar et al.

Title Page

Abstract Introduction

Conclusions References

Tables Figures

◀ ▶

◀ ▶

Back Close

Full Screen / Esc

Printer-friendly Version

Interactive Discussion



**Inverse modeling of
CO₂ sources and
sinks**

R. Nassar et al.

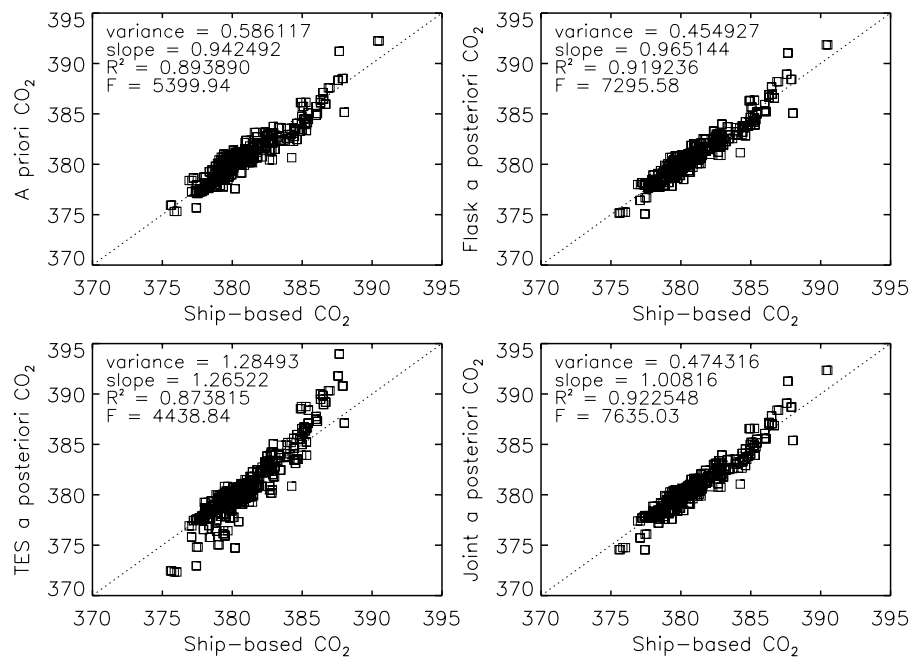


Fig. 6b. Continued.

[Title Page](#)[Abstract](#)[Introduction](#)[Conclusions](#)[References](#)[Tables](#)[Figures](#)[◀](#)[▶](#)[◀](#)[▶](#)[Back](#)[Close](#)[Full Screen / Esc](#)[Printer-friendly Version](#)[Interactive Discussion](#)